



**HAL**  
open science

## Hydration in diluted solutions of brownmillerite extracted from SR cement and synthetic brownmillerite

Alexis Mériot, sandrine Gauffinet, Marie-Noëlle de Noirfontaine, Mireille  
Courtial, Karen Alloncle, Laurent Izoret, Frédéric Dunstetter

### ► To cite this version:

Alexis Mériot, sandrine Gauffinet, Marie-Noëlle de Noirfontaine, Mireille Courtial, Karen Alloncle, et al.. Hydration in diluted solutions of brownmillerite extracted from SR cement and synthetic brownmillerite. *Cement and Concrete Research*, 2024, 181, pp.107518. 10.1016/j.cemconres.2024.107518 . hal-04571877

**HAL Id: hal-04571877**

**<https://hal.science/hal-04571877v1>**

Submitted on 9 May 2024

**HAL** is a multi-disciplinary open access archive for the deposit and dissemination of scientific research documents, whether they are published or not. The documents may come from teaching and research institutions in France or abroad, or from public or private research centers.

L'archive ouverte pluridisciplinaire **HAL**, est destinée au dépôt et à la diffusion de documents scientifiques de niveau recherche, publiés ou non, émanant des établissements d'enseignement et de recherche français ou étrangers, des laboratoires publics ou privés.

# Hydration in diluted solutions of brownmillerite extracted from SR cement and synthetic brownmillerite

Alexis Mériot<sup>1,2</sup>, Sandrine Gauffinet<sup>3\*</sup>, Marie-Noëlle de Noirfontaine<sup>1</sup>, Mireille Courtial<sup>1,4</sup>, Karen Alloncle<sup>3</sup>, Laurent Izoret<sup>2\*\*</sup> and Frédéric Dunstetter<sup>1</sup>

<sup>1</sup>Laboratoire des Solides Irradiés, CEA-DRF-IRAMIS, CNRS, Ecole Polytechnique, Institut Polytechnique de Paris, 91120, Palaiseau, France

<sup>2</sup>France Ciment, 16 bis boulevard Jean-Jaurès, 92110, Clichy, France

<sup>3</sup>Laboratoire Interdisciplinaire Carnot de Bourgogne, CNRS, Université de Bourgogne, 21078, Dijon, France

<sup>4</sup>Université d'Artois, 1230 Rue de l'Université, 62408, Béthune, France

(\*\*) Current address: Réseau Réciproque Conseil, 2 rue Torricelli, 75017, Paris, France

\*Correspondence: [sandrine.gauffinet@u-bourgogne.fr](mailto:sandrine.gauffinet@u-bourgogne.fr)

Funding information: France Ciment; Grant No. PRS/19-03 and ANRT, Grant CIFRE No. 2019/0803

Keywords: Calcium Aluminoferrite, Sulfate Resistant Cements, X-ray Diffraction, Hydration, Ettringite

Highlights:

- Characterization of the intrinsic reactivity of ferrite extracted from SRPC
- SR ferrite reactivity strongly depends on the Al/Fe ratio and medium
- Synthetic ferrites do not mimic well the real material
- Ferrite from SR0 and SR3 clinkers are distinguished only by their dissolution rate
- At early age, portlandite favors iron incorporation in katoite and ettringite

## Abstract

The aim of this study is to investigate the reactivity of ferrites extracted from Sulfate Resisting (SR) Portland cement clinkers, until now often neglected. Industrial materials and synthetic materials have been studied and compared in the whole range of the Al/Fe ratio. Highly diluted aqueous suspensions were used, ranging between pure water and more complex solutions simulating the pore solution in cement. Conductimetry was combined with ICP.

The reactivity of ferrite depends on the environment and the aluminum content of ferrite. The reactivity of ferrites extracted from industrial SR0 and SR3 clinkers ( $C_3A = 0$  wt.% and  $C_3A \leq 3$  wt.% respectively) can be distinguished from one another. Additionally, industrial ferrite was found to be more reactive than synthetic ferrite. The iron content of katoite and ettringite was investigated using XRD. It depends on the Al/Fe ratio of ferrite and the presence of calcium hydroxide in the solution.

## 1. Introduction

Sulfate Resisting Portland Cement (SRPC) have been developed to be used in sulfated environments such as sea water and gypsum-rich soil. It is well known that the aluminate phases, more precisely the  $C_3A$  phase<sup>1</sup>, play a key role in the resistance of Portland cements to external sulfate attack [1, 2]. Monosulfoaluminate, formed mainly by the  $C_3A$  hydration, reacts with the sulfate from the environment and subsequently produces expansive ettringite responsible for cracks and swelling. The  $C_3A$  content in SRPC clinkers was therefore limited in order to increase their sulfate resistance. Cement manufacturers decrease the  $C_3A$  content by decreasing the “A/F modulus” (i.e. the  $Al_2O_3/Fe_2O_3$  ratio) of the raw mix, leading to the formation of an iron-rich ferrite phase, where the Al/Fe ratio of the ferrite ranges between 0.7 and 1 [3], whereas  $Al/Fe > 1$  in ordinary Portland cement [4]. This ferrite phase, also called brownmillerite, is a wide solid solution between  $C_2F$  and  $C_6A_2F$ , often written as  $Ca_2Al_xFe_{2-x}O_5$  with  $0 < x < 1.4$ .

However, poor performances of cements with low  $C_3A$  content are sometimes observed in a highly sulfated medium, which raises the question of the intrinsic reactivity of the aluminoferrite phase in an external sulfate attack. Today, ferrite is attracting attention mainly due to the use of low  $CO_2$  cements, such as high Fe Calcium SulfoAluminate (CSA) cement, or specific applications such as high Fe Calcium Aluminate Cement (CAC) and sulfate resisting cements [5-10]. The reactivity and hydration mechanisms of brownmillerite have been widely studied on synthetic material [6, 8, 11-29]. Most of the studies only deal with a single stoichiometry of the solid solution ( $C_4AF$ , i.e.  $Al/Fe = 1$ ), which are highly representative of the ferrites found in Portland cement, but not of SR cements or sulfo-aluminate cements. Few studies have actually been devoted to the reactivity of ferrites with other values of the  $x$  parameter in the solid solution, and it is now well known that their reactivity increases with the aluminum content [6, 19-22, 24]. Nevertheless, some studies have investigated the reactivity of industrial ferrite extracted by the SAM method [30, 31].

In this paper, we have chosen to study industrial ferrites extracted from four sulfate resisting Portland clinkers ( $0.7 < Al/Fe < 1$ ) as well as a wide range of synthetic ferrites with different iron content ( $Al/Fe$  between 0 and 2). Compared to classical extraction protocols [32], we introduced a supplementary step to remove the  $C_3A$  and sulfate phases [3]. This dual approach has made it possible to compare synthetic and industrial ferrite and then determine the important factors that play a role in reactivity. Given the crucial role of aluminum contributed by the  $C_3A$  phase and considering the chemical variation in the brownmillerite composition, we can form the hypothesis that, despite the reputation of the low reactivity of ferrite, its aluminum content could play a key role in the sensitivity of brownmillerite to external sulfate. This sensitivity could be expressed by a critical value of the  $Al/Fe$  ratio (pivot value), a value which may not necessarily be equal to 1.

The aim of this paper is to investigate whether a “pivot value” exists in the reactivity of ferrite, with respect to the aluminum content. Within this context, the reactivity of synthetic and industrial ferrite was investigated by conductimetry and by Induced Coupled Plasma – Optical Emission Spectroscopy (ICP - OES) in diluted solution. During the hydration of the systems, the dissolution of anhydrous phases and the precipitation of hydrates take place simultaneously at different rates, which leads to variations in the ionic species in solution. Thus, conductimetric monitoring, depending on ionic concentrations, makes it possible to highlight the different reaction stages. In diluted condition, there is an increase in the duration of the different hydration stages, which facilitates the comparison of the different systems studied. The conductimetry method was successfully used to track the dissolution of  $C_3S$  and the nucleation of C-S-H [33-35] in diluted solution (water/cement = 400). Otherwise, investigation of cement hydration in diluted suspension enables the aqueous phase to be analyzed thoroughly. ICP – OES is also performed to monitor the calcium and aluminum concentration in a highly diluted solution (water/cement = 3000). This high water/cement ratio was chosen to prevent the precipitation of hydrated

---

<sup>1</sup> C = CaO; S = SiO<sub>2</sub>; A = Al<sub>2</sub>O<sub>3</sub>; F = Fe<sub>2</sub>O<sub>3</sub> in abbreviated stoichiometric oxide notation

phases. This method was developed by Nicoleau and Nonat and used to study the dissolution of  $C_3S$  and  $C_2S$  [36-38].

To investigate the hydration process of ferrite, industrial and synthetic ferrites were hydrated in pure water, saturated calcium hydroxide solution, saturated gypsum solution and saturated solution in calcium hydroxide and gypsum. These solutions were chosen to extend from the simplest (pure water) to the closest in terms of the cement pore solution at an early age (saturated solution in calcium hydroxide and gypsum). As a matter of fact, real cement brings to the solution both portlandite due to the calcium silicate reaction and sulfates due to the gypsum reaction.

For each type of solution, a seven-day hydration of ferrite is performed using a diluted solution (weight ratio water over cement,  $w/c = 400$ ). In pure water, in order to separate the set of reactions of ferrite from the reactions due to the presence of the solute in the three saturated solutions, we also performed a 30-minute hydration of ferrite in a very diluted solution ( $w/c = 3000$ ). In all these experiments, the hydration process was monitored using conductimetry together with ICP-OES. In parallel with these techniques, X-Ray Diffraction (XRD) was used for phase identification and quantification and for a more precise analysis of the composition in terms of iron incorporation in the solid solutions of katoite and ettringite.

## 2. Materials and methods

### 2.1. Materials

Two types of samples were used for reactivity studies:

- Synthetic ferrite with various Al/Fe ratios
- Ferrites from four commercial clinkers designated as A to D, supplied to SFIC by four plants in Europe. Two SR0 clinkers and two SR3 clinkers were used. SR0 means a cement with 0 wt.% of  $C_3A$  content and SR3 means a cement with  $\leq 3$  wt.% of  $C_3A$  content [39]. These cements contain major silicate phases ( $C_3S$  and  $C_2S$ ) which render very difficult both the interpretation of the reactions (conductimetry) and the analysis of the reaction product (ICP-OES and XRD). Therefore, dissolution methods were used in order to remove (i) the silicate compounds (SAM dissolution) and (ii) the sulfate and  $C_3A$  compounds (AcA dissolution).

#### 2.1.1. Synthetic brownmillerite

Synthetic ferrite was obtained by firing a stoichiometric mixture of  $Al_2O_3$  ( $\geq 98$  %, Sigma-Aldrich),  $Fe_2O_3$  ( $\geq 95$  %, Sigma-Aldrich,  $> 99.4\%$  measured by X-ray fluorescence spectroscopy) and  $CaCO_3$  (AnalaR NORMAPUR, VWR) for 2 h at  $1350^\circ C$  in a platinum crucible, and then quenched in air. The product was manually ground in an agate mortar and re-fired at  $1350^\circ C$  for two additional hours. Using this procedure, various synthetic samples were produced, with the Al/Fe ratio values: 0, 0.1, 0.5, 0.6, 0.7, 0.8, 0.9, and 1.

#### 2.1.2. Industrial brownmillerite: extraction by selective dissolutions

A first step of selective dissolution using Salicylic Acid/Methanol extraction (SAM) was performed in order to dissolve the calcium silicates and free lime. The concentration of ferrite in the SAM residue was much higher. However,  $C_3A$  and sulfate phases were still present. A second step of

selective dissolution using acetic acid (AcA) was used to dissolve the  $C_3A$  and sulfate phases in the SAM residue to leave mainly the ferrite phase in the residue. Quartz and periclase were still present in the AcA residue. The samples and the extraction protocols are described in [3]. The average formula of the ferrites A to D are given in Table 1. The Al/Fe ratio runs between 0.71 and 0.95. Two families could be identified: an SR0 family (A&C) with Al/Fe ratio of 0.7 and an SR3 family (B&D) with Al/Fe ratio  $\sim 0.9$ .

**Table 1**

Averaged ferrite formula from selected electron microprobe spot analysis using the SAM residue (standard deviations in parentheses). Data from ref. [3]

Clinker	Structural formula	Al/Fe
A SR0	$Ca_{2.08(4)}Mg_{0.13(1)}Al_{0.69(8)}Fe_{0.98(8)}Si_{0.14(5)}O_5$	0.71 (11)
B SR3	$Ca_{2.05(4)}Mg_{0.10(2)}Al_{0.80(16)}Fe_{0.94(7)}Si_{0.11(5)}O_5$	0.87 (24)
C SR0	$Ca_{2.11(8)}Mg_{0.16(5)}Al_{0.67(7)}Fe_{0.98(12)}Si_{0.13(6)}O_5$	0.69 (12)
D SR3	$Ca_{2.12(3)}Mg_{0.11(1)}Al_{0.80(9)}Fe_{0.87(12)}Si_{0.13(3)}O_5$	0.95 (23)

Fig. 1 illustrates the location of the industrial and synthetic ferrite compounds in the solid solution phase diagram depending on the Al/Fe ratio values. The composition of the synthetic samples was chosen to cover the whole domain of the Al/Fe ratio found for the industrial samples.

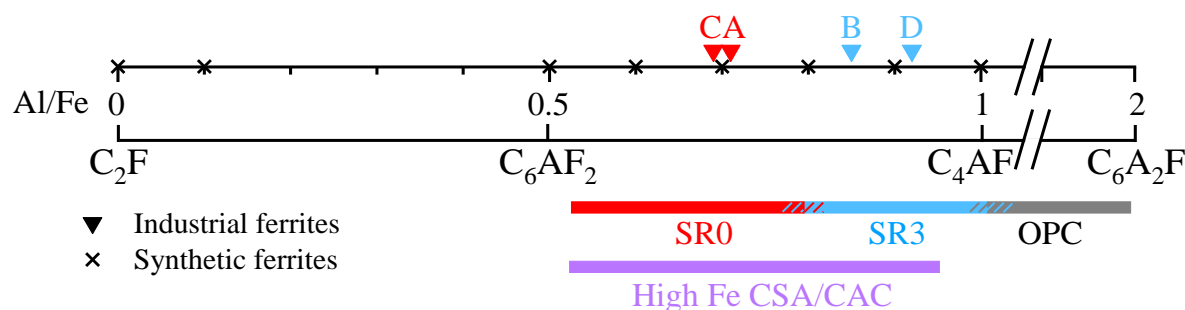


**Fig. 1.** Solid solution of ferrite; synthetic ferrites are marked with crosses and industrial ferrites are marked by triangles. Domains of ferrite composition in SR cements, OPC and High Fe CSA/CAC are reported for comparison.

## 2.2. Methods

### 2.2.1. Experimental protocol for reactivity monitoring

Pure water experiments were carried out using distilled and permuted water. A saturated  $Ca(OH)_2$  solution was prepared by dissolving pure  $Ca(OH)_2$  ( $\geq 96\%$ , Honeywell) in excess in water, and vacuum-filtered using a  $1.0 \mu m$  Millipore filter. The gypsum and gypsum/calcium hydroxide saturated solutions were obtained by the same protocol using  $CaSO_4 \cdot 2H_2O$  (NORMAPUR, Prolabo). Ferrite hydration was followed by conductimetry over seven days. The solutions were then vacuum-filtered

again using a 1.0  $\mu\text{m}$  Millipore filter. The residue was washed out with isopropanol to stop the hydration process. The residue was then stored in a vacuum desiccator and subsequently analyzed by XRD. The filtrate was kept for later ICP-OES analysis. In very diluted aqueous solution ( $w/c = 3000$ ), the protocol was somewhat different. The experimental setup for the monitoring of the ionic concentration is described in [36]. The powder was diluted in stirred water. The evolution of the ionic concentration was tracked by ICP-OES every 30 seconds for 20 to 30 minutes.

### 2.2.2. Conductimetry

The conductivity of the solutions was recorded by a 2-pole conductivity cell (Radiometer Analytical) calibrated with a  $0.1 \text{ mol.l}^{-1}$  KCl solution at  $25^\circ\text{C}$ . All conductivity measurements were made at  $25^\circ\text{C}$  in a 400 ml reactor over 7 days. To avoid carbonation, a flow of  $\text{N}_2$  is ensured in the closed reactor. The solution is stirred (about 200 rpm) with a magnetic stir bar.

### 2.2.3. ICP-OES

ICP-OES measurements were performed on a 5110 Agilent Technologies spectrometer. The following wavelengths were used to measure the concentrations: Al (226.346 nm; 237.312 nm; 257.509 nm; 308.215 nm; 396.152 nm), Ca (210.324 nm; 211.276 nm; 431.865 nm; 445.478 nm; 643.907 nm) and S (181.972 nm; 182.562 nm). Filtrates were acidified by 1%  $\text{HNO}_3$ .

### 2.2.4. XRD

XRD data were collected using a powder X-ray diffractometer (D8 Advance, Bruker AXS, Karlsruhe, Germany) in the Bragg-Brentano geometry ( $\theta/\theta$ ). The instrument was operated in step-scan mode (steps: 1s,  $0.005^\circ$  in  $2\theta$ ), between  $5^\circ$  and  $90^\circ$ . To minimize preferential orientation, the powder was prepared by backloading. Phase identification was performed using DIFFRAC.EVA software (version 5, Bruker-AXS, Karlsruhe, Germany, 2010–2020). Rietveld refinements were performed using TOPAS software (version 6, Bruker-AXS, Karlsruhe, Germany, 1999–2016) based on the fundamental parameters approach [40]. The starting structural models used for the refinements are given in Table 2. The refined parameters included scale factor, sample displacement, coefficients of the background described as a fifth-order Chebychev polynomial combined with a  $1/X$  term, unit cell parameters, and crystallite size (referred to as  $L_{\text{vol-IB}}$ ). The atomic positions and temperature factors of all phases were kept constant in the crystal structures. Preferred orientation was corrected using the March-Dollase algorithm [41] for the ettringite 100 Bragg lines. For the ferrite phase, additional refined parameters were added: a strain parameter (referred to as strain G) and the occupancy factors of aluminum and iron on tetrahedral and octahedral sites. For katoite, the occupancy factors of aluminum and iron on octahedral sites were also refined.

**Table 2**

Phases of clinkers, SAM, and AcA residues: structural data, PDF and ICSD file numbers. For each phase, the ICSD codes (Inorganic Crystal Structure Database, web version 1.1.0) and PDF numbers (International Centre for Diffraction Data (ICDD) PDF, release 2002) are provided for information. The PDF number in parentheses corresponds to experimental data.

Phase/mineral name	Formula	Symmetry	Space group	PDF file	ICSD	Reference
$C_4AF$ Brownmillerite	$Ca_2AlFeO_5$	Orthorhombic	<i>Ibm2</i> (46)	01-071-0667 (00-030-0226)	9197	[42]
$C_2F$ Srebrodolskite	$Ca_2Fe_2O_5$	Orthorhombic	<i>Pcmn</i> (62)	01-071-2108 (00-038-0408)	14296	[43]
Cubic $C_3A$ Tricalcium aluminate	$Ca_3Al_2O_6$	Cubic	<i>Pa-3</i> (205)	01-070-0839 (00-038-1429)	1841	[44]
Katoite	$Ca_3Al_2(OH)_{12}$	Cubic	<i>Ia-3d</i> (230)	01-073-9982 (00-024-0217)	82404	[45]
Ettringite	$Ca_6Al_2(SO_4)_3(OH)_{12}.26(H_2O)$	Trigonal	<i>P31c</i> (159)	(00-041-1451)	155395	[46]
Calcium monosulfoaluminate	$Ca_4Al_2(OH)_{12}(SO_4).6(H_2O)$	Trigonal	<i>R-3</i> (148)	83-1289	100138	[47]
Gypsum	$CaSO_3.2(H_2O)$	Monoclinic	<i>C12/c</i> (15)	01-071-2701 (00-033-311)	409581	[48]

### 2.2.5. Specific area BET and SEM analysis

Specific surface area was determined using the physical adsorption of nitrogen or krypton (for surfaces less than  $10,000 \text{ cm}^2.\text{g}^{-1}$ ) within the BET method. Before the measurement, samples were outgassed for one hour at  $400^\circ\text{C}$ . The measurements were performed at  $-196^\circ\text{C}$  using a Micromeritics TriStar II coupled to a Micromeritics Smart VacPrep. Samples were investigated with a Scanning Electron Microscope (SEM) HITACHI S 4800 on a carbon tape.

## 3. Ferrite hydration

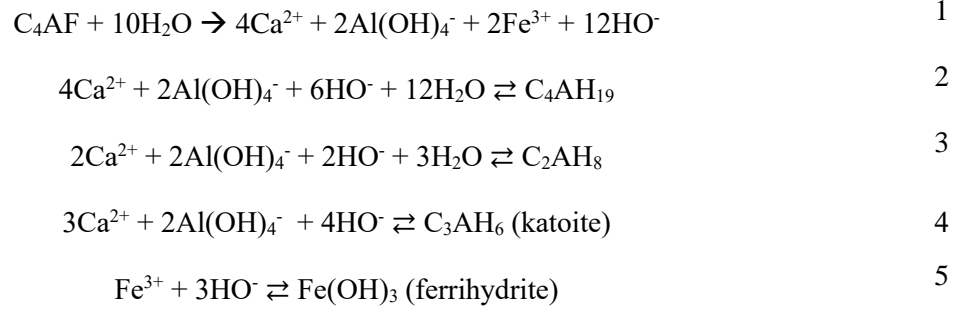
This part discusses, according to the literature, the hydration reactions of ferrite in water, sulfated solution, and carbonated solution. This will introduce the incorporation of iron in the hydrates.

Pure water:

The classic hydration reactions of ferrite in pure water solution are well known. They produce various hydrates, depending on the equilibrium between calcium, aluminum, and iron. The hydrates formed by the hydration process of ferrite and the hydration process of  $C_3A$  are very similar, despite a significant discrepancy in the kinetics of their reactions. To simplify the following equations, ferrite is approximated to  $C_4AF$ . The first step in the hydration process of ferrite is a partial congruent dissolution (equation 1). However, Tao et al. [49] have shown at the atomic scale that during the hydration process the attack on the tetrahedral sites occupied by aluminum is faster than on the octahedral sites occupied by iron. The increasing concentration of ions then allows the precipitation of hydrates. As for  $C_3A$ , the first hydrates precipitate as hexagonal plates,  $C_2AH_8$  and  $C_4AH_{19}$ , formed within 5 minutes (equations 2 and 3) [24]. The  $C_2AH_8$  and  $C_4AH_{19}$  hydrates are unstable, and they dissolve and then precipitate as a cubic shaped hydrate ( $C_3AH_6$ ) after 24h (equation 4). This process is quite slow, and hexagonal plates can still be observed after 4 months. The chemical formula of cubic hydrates is  $C_3AH_6$ , also designated

as hydrogarnet or katoite. These equations for the hydration process of ferrite are strictly identical to the  $C_3A$  hydration reactions. However, in this case we consider that all the iron ions are contained in the  $Fe(OH)_3$  precipitating gel, also called ferrihydrite (equation 5).

In saturated calcium hydroxide solution, the hydration process is strictly identical. Precipitation of the  $C_4AH_{19}$  phase is favored compared to the  $C_2AH_8$  phase.

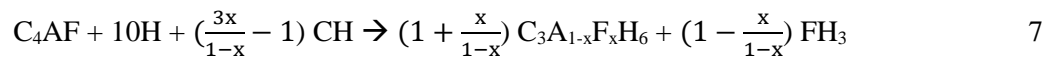


Katoite is the main hydrated phase of ferrite in the absence of sulfates. Katoite is a hydrogarnet which is part of the quaternary diagram  $C_3AH_6 - C_3AS_3 - C_3FH_6 - C_3FS_3$ . The hydrogrossular solid solution  $Ca_3Al_2(SiO_4)_{3-x}(OH)_{4x}$  has been studied in depth [50, 51]. This is not the case for the  $C_3AH_6 - C_3FH_6$  domain, which is still subject to discussion. Dilnesa et al. [52] have shown the lack of a solid solution between  $C_3AH_6$  and  $C_3FH_6$ . However, katoite containing iron was often confirmed, where the Al/Fe ratio is always lower than in ferrite [12, 15, 18, 19, 26, 27, 53-55]. Usually, the formula of katoite which results in the hydration of  $C_4AF$  is  $C_3A_{0.845}F_{0.155}H_6$  [15]. The most complete work on the incorporation of iron in katoite was reported by Taylor [4], leading to an empirical formula estimating the iron and silica content in katoite, starting from its cell parameter (equation 6). This formula was also used by [55] to estimate the iron substitution in katoite from an SR cement:

$$a \text{ (\AA)} = 11.71 + 0.16x + 0.144y \quad 6$$

where  $x = [Fe_2O_3]$  and  $y = [H_2O]$  are the coefficients of the stoichiometric formula  $C_3A_{1-x}F_xS_{3-y/2}H_y$  of the solid solution.

Incorporation of iron in hydrates strongly depends on the nature of the solution. Several authors have observed that hydrates obtained in calcium hydroxide solution or in the presence of  $C_3S$  have a higher iron content than those obtained in pure water [18, 20, 54]. It is Perez's work which first demonstrated that the iron content in the hydrate depends on the portlandite content [27]. The hydration process of ferrite with portlandite can be written thus (equation 7):

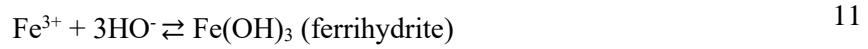
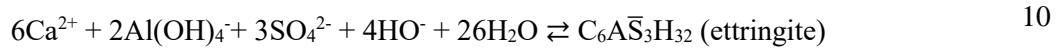
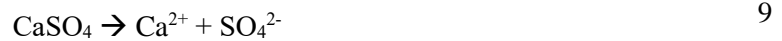
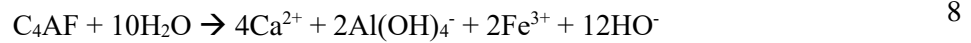


where  $x$  ranges between 0 and 0.5. This equation will determine iron incorporation in katoite. For  $x$  between 0 and 0.25, portlandite is not a reactant but a product of the reaction, and the iron incorporation remains weak. For  $x$  between 0.25 and 0.5, portlandite becomes a reactant: iron incorporation is strong.



Sulfated water:

In the presence of sulfate, the hydration process of ferrite is very different regarding the nature of precipitated hydrates. Anhydrite (CaSO<sub>4</sub>) has been chosen to describe the hydration process, but the mechanism remains valid for any other source of sulfate. As previously, the first step is a dissolution of ferrite (equation 8) and anhydrite (equation 9). The main hydrate that precipitates is ettringite Ca<sub>6</sub>Al<sub>2</sub>(SO<sub>4</sub>)<sub>3</sub>(OH)<sub>12</sub>·26H<sub>2</sub>O (C<sub>6</sub>A $\bar{S}$ <sub>3</sub>H<sub>32</sub>) (equation 10). The “AFT” notation is often used to designate ettringite, even if it is a general notation for every tri-substituted hydrate. Fe(OH)<sub>3</sub> gel also precipitates (equation 11).



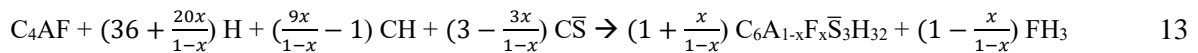
When the sulfate content in solution is not sufficient, ettringite is not stable. It first dissolves and later precipitates in the form of calcium monosulfoaluminate C<sub>4</sub>A $\bar{S}$ H<sub>12</sub> (equation 12) [56].



Several authors have investigated the iron incorporation in ettringite. Emanuelson confirmed by Energy-Dispersive X-ray (EDX) analysis the iron incorporation in ettringite, with the stoichiometric formula Ca<sub>6</sub>[Al<sub>0.5</sub>Fe<sub>0.5</sub>(OH)<sub>6</sub>]<sub>2</sub>(SO<sub>4</sub>)<sub>3</sub>·26H<sub>2</sub>O resulting from ferrite hydration [54]. Fukuhara [26] estimated that ettringite is substituted in iron by about 25% after ferrite hydration.

The most complete work on iron incorporation in ettringite was done by Renaudin [57] and Möschner [58]. Möschner showed that the Al-Fe-ettringite solid solution is not continuous, with a miscibility gap between x = 0.3 and x = 0.6, where x is the coefficient in the Ca<sub>6</sub>[Al<sub>1-x</sub>Fe<sub>x</sub>(OH)<sub>6</sub>]<sub>2</sub>(SO<sub>4</sub>)<sub>3</sub>·26H<sub>2</sub>O stoichiometric formula.

Equation 7 states that iron in katoite depends on the portlandite content in solution. A similar reasoning can be applied to the C<sub>4</sub>AF hydration in a sulfated environment which leads to equation 13:

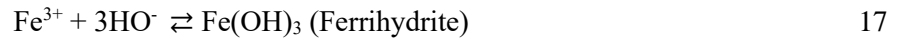
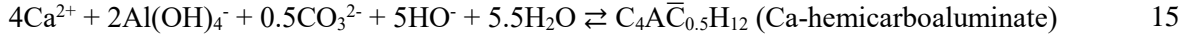


where x ranges between 0 and 0.5.

Carbonated water:

This issue is in fact more complex due to the presence of CO<sub>2</sub> and carbonates in the atmosphere and soils. In this case, parasitic reactions discussed below occur between the carbonates and the ferrite (equations 14 – 18). Whatever the efforts, it appears quite impossible to avoid them. In a carbonated solution, ferrite first dissolves (equation 14), and calcium hemi-carboaluminate precipitates (equation 15). However, this calcium hemi-carboaluminate is unstable and subsequently dissolves and then the

monocarboaluminate precipitates (equation 16). In parallel with these reactions, iron can precipitate into  $\text{Fe}(\text{OH})_3$  hydrate (equation 17) or into iron monocarbonate, also called Fe-monocarbonate, with a different water stoichiometry:  $\text{Ca}_4\text{Fe}_2(\text{OH})_{12}(\text{CO}_3)(\text{H}_2\text{O})_6$  (equation 18). Unlike other hydrates, the recent work of Dilnesa [59] shows that no solid solution exists between Al and Fe-monocarbonate.



All the reactional routes discussed here are summarized in Fig. 2.

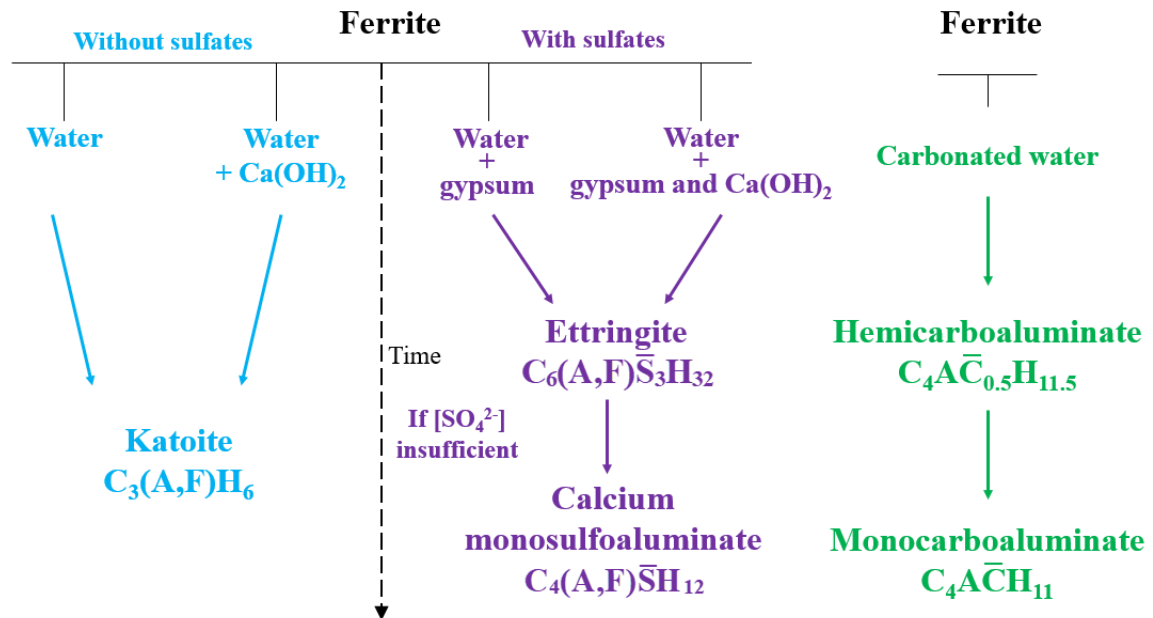


**Fig. 2.** Hydration products of ferrite in different solutions: without sulfate (in pure water and calcium hydroxide solution), with sulfate (in gypsum and in gypsum and calcium hydroxide saturated solution) and in carbonated system; Katoite:  $\text{Ca}_3\text{Al}_2\text{H}_{12}\text{O}_{12}$ ; Ettringite:  $\text{Ca}_6\text{Al}_2(\text{OH})_{12}(\text{SO}_4)_3 \cdot 26\text{H}_2\text{O}$ ; Calcium monosulfate:  $\text{Ca}_4\text{Al}_2(\text{OH})_{12}\text{SO}_4 \cdot 6\text{H}_2\text{O}$ ; Hemicarboaluminate:  $\text{Ca}_4\text{Al}_2(\text{OH})_{13}(\text{CO}_3)_{0.5}(\text{H}_2\text{O})_5$ ; Monocarboaluminate:  $\text{Ca}_4\text{Al}_2(\text{OH})_{12}(\text{CO}_3)(\text{H}_2\text{O})_5$

#### 4. Results and discussion

Using the same material, either synthetic or industrial, the four hydration routes as defined in Fig. 2 were investigated.

#### 4.1. Ferrites before hydration

Synthetic samples were analyzed by XRD to validate the purity of the material and to measure the unit cell parameters (Table 3). All samples are free from other phases.

**Table 3**

Rietveld refinement of the synthetic ferrites XRD patterns: unit cell parameters and criteria of fit (weighted-profile  $R_{wp}$  factor and  $R_{Bragg}$  factor and Goodness Of Fit - GOF). Errors for the lattice parameters are estimated standard deviations from the refinement.

Al/Fe target	Al/Fe refined	a (Å)	b (Å)	c (Å)	Volume (Å <sup>3</sup> )	Rwp	R-Bragg	GOF
0	0	5.59888 (4)	14.7673 (1)	5.42808 (3)	448.79 (1)	12.12	7.87	2.06
0.1	0.19	5.5889 (2)	14.7287 (6)	5.4199 (2)	446.16 (3)	18.22	9.35	4.17
0.5	0.58	5.5755 (2)	14.6065 (5)	5.3796 (1)	438.11 (2)	14.92	6.98	3.36
0.6	0.61	5.5734 (2)	14.5926 (5)	5.3725 (2)	436.94 (2)	12.81	5.30	3.11
0.7	0.78	5.5695 (1)	14.5738 (4)	5.3670 (1)	435.63 (2)	13.09	5.20	3.07
0.8	0.87	5.5651 (1)	14.5589 (4)	5.3602 (1)	434.29 (2)	11.83	4.76	2.83
0.9	0.89	5.5622 (1)	14.5462 (3)	5.3547 (1)	433.24 (2)	10.32	3.67	2.49
1	0.99	5.5569 (1)	14.5237 (3)	5.3484 (1)	431.95 (2)	9.60	3.44	2.35

Industrial ferrites are produced by quenching the liquid phase in the air-cooler at the outlet of the cement kiln (1450°C), whereas synthetic ferrites are produced by solid-state reaction route (1350°C). Consequently, the differences observed between industrial and synthetic ferrites concerning the chemical composition and the microstructure will influence the reactivity. Several parameters may be highlighted:

- Silica and magnesium, found in industrial ferrites, can play a role in the hydration process [60].
- The synthesis temperature plays a role in cement phases hydraulicity and ought to be taken into account in the reactivity studies [61, 62].
- The most important parameter is the specific area, to which the dissolution rate is proportional. BET measurements have shown a specific surface area of  $\sim 2,000 \text{ cm}^2 \cdot \text{g}^{-1}$  for synthetic ferrites and above  $60,000 \text{ cm}^2 \cdot \text{g}^{-1}$  for the four industrial ferrites (AcA).

#### 4.2. Hydration of ferrite with pure water

In pure water, the main hydrated phase of ferrite is katoite. Two experiments were performed. In the first, the whole process of hydration was monitored for a seven-day period with  $w/c = 400$ . Next, extra attention was given to the first periods of dissolution prior to any precipitation, using measurements at 30-minute intervals in diluted aqueous solution with  $w/c = 3000$ .

##### 4.2.1. Hydration of ferrite over seven days ( $w/c = 400$ )

###### 4.2.1.1. Synthetic ferrites

The conductivity behavior depends on the Al/Fe atomic ratio. Let us consider an intermediate value of the Al/Fe ratio (Fig. 3A, Al/Fe = 0.7). At the beginning, the conductivity regularly increases, which corresponds to the initial dissolution process of ferrite. XRD analysis at this point does not

indicate the presence of hydrated phases. The evolution of conductivity shows a decrease due to the reduction of the solubility equilibrium deviation of ferrite. As the dissolution prevails in the first part of the reaction process, the initial slope of the conductivity as a function of time can be considered as a function of ferrite dissolution. The value of the slope of conductivity as a function of the Al/Fe ratio is plotted in Fig. 4. It increases linearly. The same then applies for the dissolution speed. Similar results have been found by Carlson during the first hour of hydration [19].

Next, at a given time  $t_i$ , which we shall refer to as the inversion time, the conductivity reaches a maximum value, then decreases quite steeply and finally tends to plateau. The fall in conductivity corresponds to the massive hydrates precipitation process. **Fig. 3A** shows that the inversion time  $t_i$  depends enormously on the Al/Fe ratio. Three trends of curves can be observed in **Fig. 3A**:

- Trend 1: Neither dissolution nor precipitation; the curves remain quite flat (Al/Fe = 0 and 0.1).
- Trend 2: The dissolution process is slow and the inversion time is still not attained after seven days (Al/Fe = 0.5 and 0.6).
- Trend 3: The inversion time  $t_i$  is about one to two days; these values are not really reproducible due to numerous other experimental parameters (Al/Fe = 0.7, 0.8, 0.9 and 1).

Two domains are observed. With low aluminum content in ferrite (trends 1 and 2), the reactivity remains rather low, whereas it increases strongly above an Al/Fe value of about 0.7, this value then appearing as a pivot value of the reactivity. Low Al concentration values in solution indicate that the system is very close to hydrate solubility (**Table 4**).

#### 4.2.1.2. Industrial ferrite – SAM residues

The SAM residue contains either ferrite and/or sulfates and  $C_3A$  [3]. Ferrite and  $C_3A$  behave in the same way in pure water and with sulfates. Therefore, the presence of  $C_3A$  hides the ferrite reactivity and makes it difficult to interpret since the very origin of the final katoite in the solution is not clear. Moreover, the small sulfate amount contained in the SAM residue changes the reaction kinetics by replacing the katoite production of the ferrite with production of ettringite. For all these reasons, it appears necessary to remove both sulfates and  $C_3A$  to prevent ettringite production. The AcA dissolution process makes this possible.

#### 4.2.1.3. Industrial ferrite – AcA residues

The conductivity as a function of time for synthetic ferrites and AcA residues is plotted in Fig. 3A and **Fig. 3B** respectively. Phases identified by XRD and ionic concentrations in the solution are given in Table 4. In pure water, all the AcA residues are totally hydrated within seven days, no anhydrous ferrite remains, and the main hydrated phase is katoite (**Table 4**). Looking at the conductivity behavior, it appears to be very similar to trend 3 as defined in the previous paragraph, with competition between the precipitation and hydration processes. Diffraction experiments give Al/Fe ratio values in the range 0.7 to 0.9, also consistent with the values found for the synthetic ferrites with Al/Fe ratio from 0.7 to 1 (trend 3). Another important effect is the specific surface area. Here, the specific surface area is greater than in synthetic compounds, with the result of enhancing the reactivity.

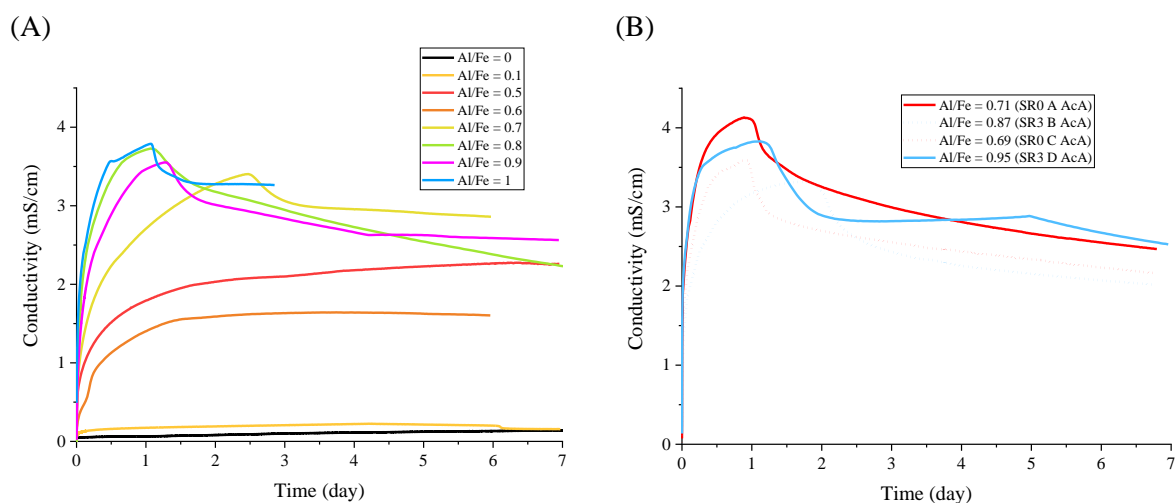


**Fig. 3.** Conductivity measurements of synthetic ferrites (A) and AcA residues (B) hydrated in pure water, w/c = 400

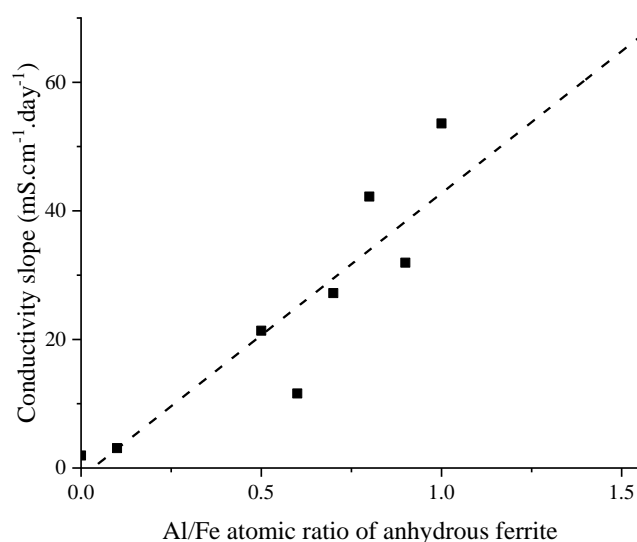


**Fig. 4.** Conductivity slope from data of Fig. 3A in the first hour of synthetic ferrites hydrated in pure water as a function of the Al/Fe atomic ratio of anhydrous ferrite

**Table 4**

Phases identified by XRD, together with Ca and Al concentrations after 7 days in pure water and calcium hydroxide solution. AcA residues and synthetic ferrites, w/c = 400; XXX: major phase; X: identified

	Al/Fe	0	0.1	0.5	0.6	0.69 (C)	0.7	0.71 (A)	0.8	0.87 (B)	0.9	0.95 (D)	1
Pure water	Anhydrous ferrite	XXX	XXX	XXX	XXX	-	X	-	-	-	-	-	-
	Hydrate	-	-	-	-	XXX	XXX	XXX	XXX	XXX	XXX	XXX	XXX
	Katoite $C_3AH_6$	-	-	-	-	XXX	XXX	XXX	XXX	XXX	XXX	XXX	XXX
	Concentration Ca (mmol/l)	0.07	0.43	2.83	3.94	4.79	3.82	4.60	3.61	4.25	2.94	4.03	4.08
Concentration Al (mmol/l)	—	0.03	1.34	2.10	0.68	0.45	0.46	1.03	0.91	1.25	0.57	1.21	

Calcium hydroxide solution	Anhydrous ferrite	XXX	X	-	-	-	-	X	X	X	X	-	-
	Hydrate	-	XXX	XXX	XXX	XXX	XXX	XXX	XXX	XXX	XXX	XXX	XXX
	Katoite $C_3AH_6$	16.60	14.71	20.16	15.33	10.46	13.68	13.04	14.66	12.84	14.31	12.67	9.69
	Concentration Ca (mmol/l)	—	0.12	Very low	0.76	Very low	0.79	Very low	1.01	Very low	0.91	Very low	0.10
Concentration Al (mmol/l)													

#### 4.2.1.4. Carbonation

Despite performing the reaction in pure water under  $N_2$  atmosphere, some carbonation can be observed due to the pollution of atmospheric carbon dioxide. In addition to the expected katoite, several carbonate hydrates can also be observed, depending on the stoichiometry: monocarboaluminate and hemicarboaluminate. A specific problem is raised with monocarboaluminate. XRD patterns exhibit two characteristic Bragg lines for the Al-monocarbonate and the Fe-monocarbonate. But between these two lines, an additional intermediate line can be observed ( $11.4^\circ$   $CuK\alpha$ ), clearly related to a mixed compound (Fig. 5). This compound has already been discussed by Dilnesa et al. [59], who referred it as  $Mc^*$ . All these phases are hereinafter referred to as “carbonates”. In addition to the observed preferential orientation, the lack of structural model renders the quantitative analysis by XRD very difficult.

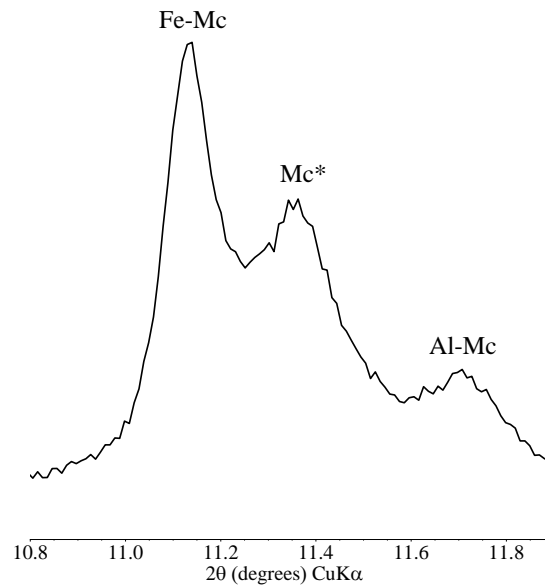


**Fig. 5.** Fe-monocarbonate,  $Mc^*$  and Al-monocarbonate signatures [59] in  $C_4AF$  (Al/Fe = 1) hydrated 7 days in a calcium hydroxide solution.

#### 4.2.2. Dissolution in water: $w/c = 3000$

As shown previously, the monitoring of the conductivity gives precious information regarding the ferrite hydration process. However, it is impossible to distinguish industrial ferrites from one another. To overcome this drawback, the dissolution rate of residues was monitored by ICP measurement of ion concentrations in a very diluted solution ( $w/c = 3000$ ). Such a high water to solid ratio is chosen to avoid precipitation of hydrated phases [36]. The evolution of the concentrations during the dissolution of SAM and AcA residues is displayed in Fig. 6 (trend 2 as defined previously).

SAM residues not only contain ferrite, but also  $C_3A$  and alkaline sulfates, which dissolve in water, bringing additional ions into the solution. We observe an intense fluctuation of calcium concentration in the first two minutes for SAM residue A (Fig. 6A). To explain this fluctuation, we raise the hypothesis of an initial dissolution of the calcium sulfates contained in the SAM residue A, followed by fast precipitation. Concentration monitoring of AcA residue A (Fig. 6C) shows a similar phenomenon but on a smaller scale. For the SAM residues B and D, the high  $C_3A$  concentration, respectively 8.5 and 11.1 wt.%, renders the data interpretation rather difficult, due to the faster dissolution rate of  $C_3A$  compared to ferrite, as already known [30, 63, 64]. The very sharp decrease in the concentration at some points is an artefact of the measurement due to air bubbles in the spectrometer's tubes.

Looking at Fig. 6, one can observe that the evolutions of aluminum and calcium concentrations both exhibit asymptotic values, for both SAM and AcA residues. The asymptotical concentrations are systematically higher for SR3 than for SR0 clinkers. The two SR0 and SR3 families of curves are well separated, with similar behavior of the two samples in each family. This derives from the higher Al/Fe ratio in the SR3 compounds, which induces a higher dissolution. It was possible to observe this phenomenon thanks to the very high w/c ratio that highlights the distinction between the two families. The dispersion of the data is higher for the SAM samples than for the AcA samples due to the contribution of the ions arising from  $C_3A$  and sulfates, which partially masks the contribution of ferrite. Therefore, the AcA samples were used for our conductivity studies. As far as Electron Probe Micro Analysis [3] made it possible to distinguish SR0 from SR3 clinkers, it appears here that this simple chemical method is also able to distinguish these two types of compounds.

In the foregoing, the discussion has been restricted to calcium and aluminum ions. The reason is that, in all our experiments, iron was never detected by ICP, for its concentration remains very low. A hypothesis is the immediate precipitation of  $FH_3$  gel as soon as iron appears in the solution. This is consistent with the value of the precipitation constant  $pK_s$  2.6 [59], which implies that for a pH value of 12, only  $3 \times 10^{-2}$  mmol of  $Fe(OH)_4^-$  is needed for  $Fe(OH)_3$  precipitation.

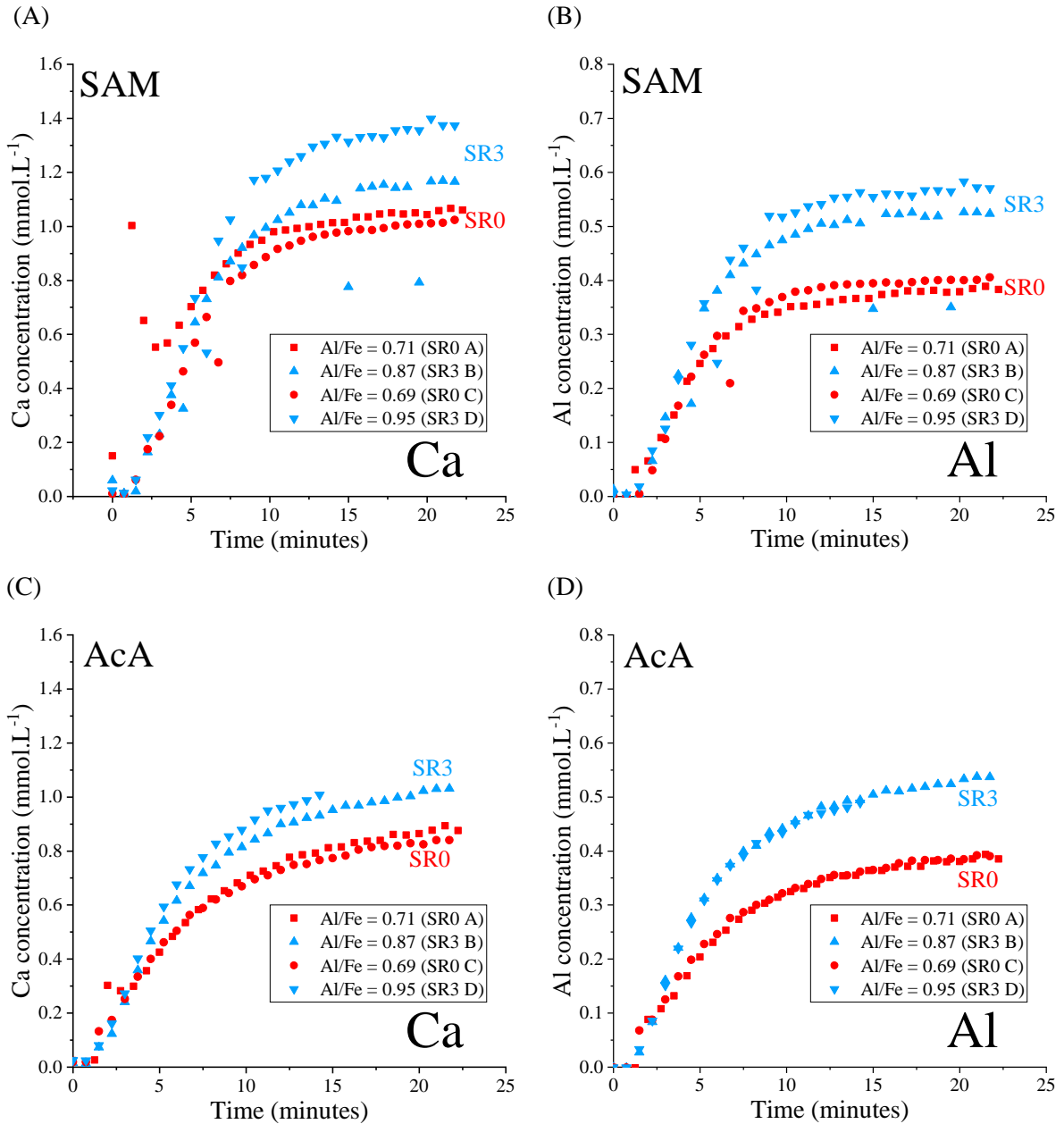


**Fig. 6.** Evolution of Al and Ca concentrations as a function of time for residues SAM and AcA in pure water,  $w/c = 3000$

#### 4.3. Hydration of ferrite with calcium hydroxide solution

A simplified equation of  $C_4AF$  hydration in calcium hydroxide solution is given by equation 7, where  $x$  is related to iron incorporation in katoite ( $C_3A_{1-x}F_xH_6$ ). Ferrite reactivity was then studied in water saturated with calcium hydroxide without a solid supply source. This solution was used so as to be closer to the hydration of ferrite in a cementitious matrix. The high concentration of  $Ca^{2+}$  and  $HO^-$  ions will promote  $C_4AH_{19}$  precipitation over  $C_2AH_8$  precipitation. It will also decrease the amount of aluminum ions needed for hydrated phase precipitation. As for pure water, ferrite hydration was monitored by conductimetry with  $w/c = 400$ . Conductivity as a function of time for ferrites in calcium hydroxide solution is displayed in Fig. 7. For all ferrites, conductivity decreases over time, except for  $C_2F$ , for which conductivity remains constant. The decrease is more pronounced for ferrite with  $Al/Fe$  ratio = 1 than for ferrites with low  $Al/Fe$  ratios (i.e. 0.1). The decrease in conductivity can be explained



by a decrease in the concentration of conductive species, arising from  $\text{Ca}^{2+}$  and  $\text{HO}^-$  consumption, which is confirmed by the concentration values (**Table 4**).

For  $x$  values over 0.25, portlandite is consumed, with strong iron incorporation in katoite. In the opposite case ( $x < 0.25$ ), the excess of calcium in ferrite compared to  $\text{C}_3\text{A}$  leads to portlandite CH production. The conductivity should then increase along with the pH and calcium concentration. This, however, is not observed, and the decrease in conductivity observed in Fig. 7 seems to indicate a strong iron incorporation in katoite ( $x > 0.25$ ).

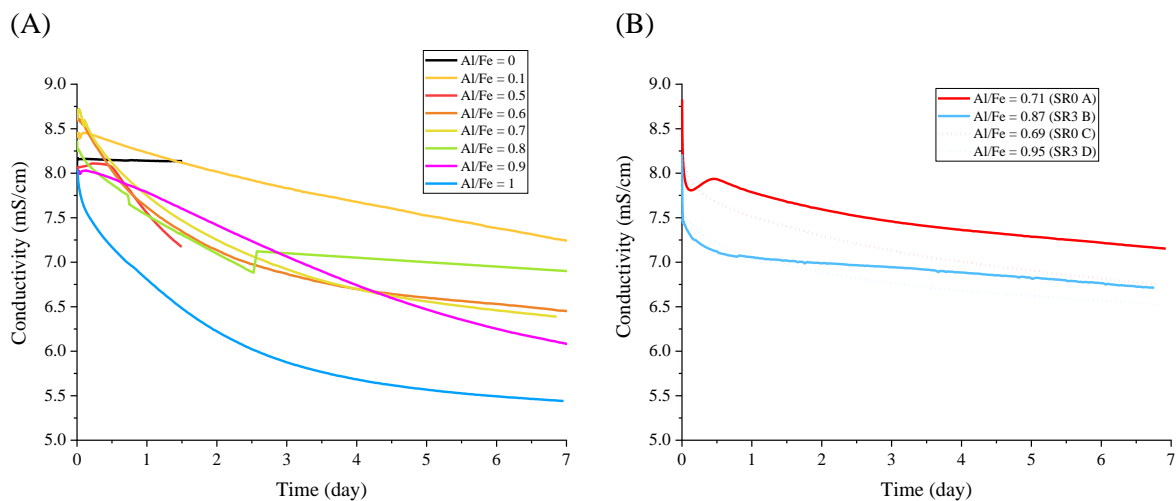


**Fig. 7.** Conductivity measurements of synthetic ferrites (A) and AcA residues (B) hydrated in calcium hydroxide solution,  $w/c = 400$

As in pure water, Rietveld quantification is impossible owing to the presence of carbonates. However, in our samples, all the ferrites were hydrated into katoite, except  $\text{C}_2\text{F}$  ( $\text{Al/Fe} = 0$ ) which remains unhydrated (Fig. 8). As soon as the ferrite contains aluminum, hydration is observed.

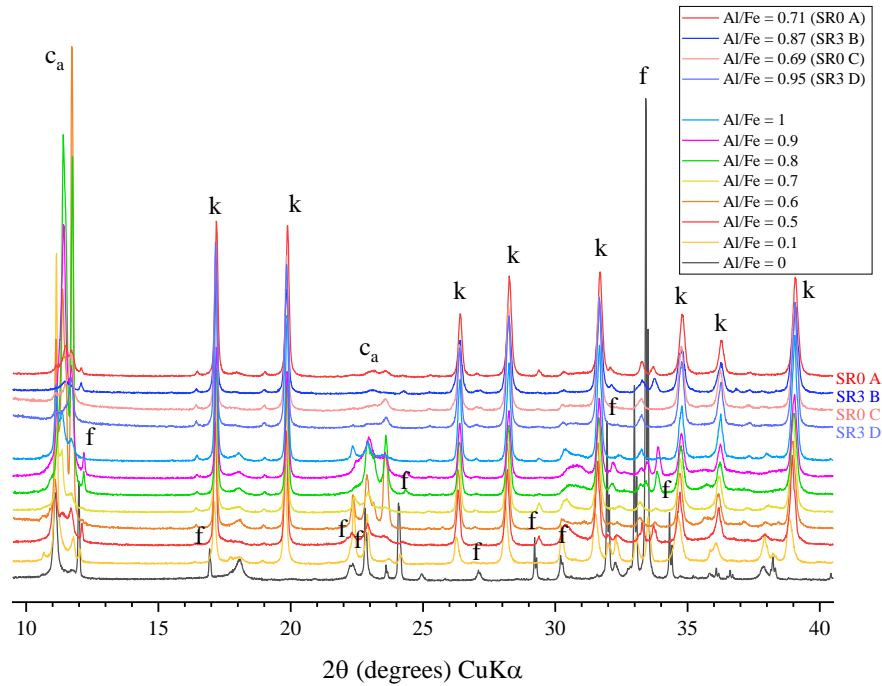


**Fig. 8.** XRD patterns of synthetic ferrites and AcA residues hydrated for 7 days in calcium hydroxide solution (f: ferrite, k: katoite, c<sub>a</sub>: carbonates)

#### 4.4. Al-Fe-Si katoite solid solution

As seen previously, the hydration of ferrite in water, with or without portlandite, mainly produces katoite. In this paragraph, we will discuss in more detail the stoichiometry of katoite as a function of the iron content of the initial ferrite sample. Another point is the incorporation in katoite of the silicon existing as an impurity in the ferrite of a clinker.

##### 4.4.1. Incorporation of iron

Here, we mainly used XRD, capable of giving precise values of the unit cell parameter of the cubic katoite. As seen previously, Taylor gave a linear formula (eq. **Erreur ! Source du renvoi introuvable.**) between the unit cell parameter and the iron content of the ferrite, i.e. the x parameter of the stoichiometric formula of katoite  $C_3A_{1-x}F_xH_6$ . This dependence of the unit cell parameter on the iron content is related to the difference between the ionic radius of the aluminum and iron ions (0.645 Å for  $Fe^{3+}$  vs 0.535 Å for  $Al^{3+}$  in octahedral coordination) [65]. When silicon is also present in katoite, a modification of this Taylor formula becomes necessary. The variation of the unit cell parameter was measured by XRD as a function of the Al/Fe ratio in various samples (Fig. 9). The behavior in pure water and in calcium hydroxide solution is very different. The unit cell parameter of katoite is shorter (0.5%) in pure water than in calcium hydroxide solution and corresponds to the value for katoite close to the stoichiometry  $C_3AH_6$ , with a low iron content. For ferrite samples of formulas close to  $C_4AF$ , a fluctuation is observed in the iron content of the katoite (x close to 0)<sup>2</sup> within the limits of validity of the Taylor formula. It can be noted that in pure water the Rietveld refinement of the site populations in

<sup>2</sup> For other compositions of ferrite, a single sample was available, but the high precision of unit cell measurements makes it possible to state an x value very close to 0, within the validity of Taylor's formula.

iron and aluminum predicts an iron content higher than the Taylor formula prediction. Conversely, the iron concentrations in the two approaches are consistent with hydration in calcium hydroxide solution. In this case, a quasi-linear variation of the katoite iron content is observed as a function of the initial ferrite iron content, with a fluctuation similar to that observed in pure water with  $C_4AF$ , as already discussed. Another point is that the katoite iron content is higher in calcium hydroxide solution than in pure water ( $x$  in the range 0.4 to 0.6 compared to close to 0).

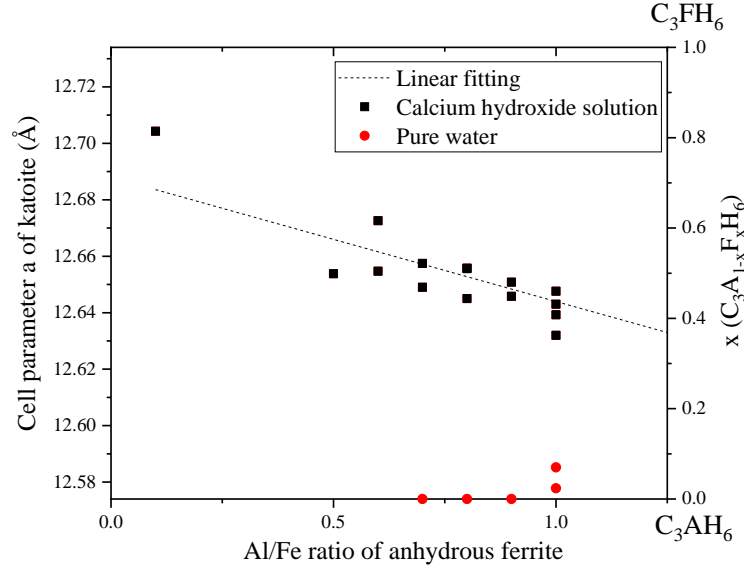


**Fig. 9.** Cell parameter  $a$  of katoite and amount of iron incorporated in katoite calculated from Taylor's formula as a function of the Al/Fe atomic ratio of ferrite

#### 4.4.2. Incorporation of silicon

All the elemental analyses performed on industrial ferrites (X-Ray Fluorescence Spectroscopy, microprobe) exhibit a non-negligible silicon content, with about 3 wt.%  $SiO_2$  [3]. This silicon is localized as a constituent, inside the ferrite unit cell. The same applies after hydration, since silicon becomes a constituent of the unit cell of katoite, where a  $SiO_2$  formula replaces two water molecules [50]. No independent hydrated silicate is observed. It becomes interesting to transpose the analysis made below now including silicon. Then, the stoichiometric formula  $C_3A_{1-x}F_xH_6$  of katoite becomes (equation 19):



where  $y$  is the  $SiO_2/Al_2O_3$  molar ratio of ferrite and  $x$  is the iron substitution.

Taylor's formula needs to be modified as (equation 20):

$$x = \frac{a - 12.574 + 0.288 y}{0.16 + 0.288 y} \quad 20$$

where  $a$  is the cell parameter of katoite.

**Table 5** gives the unit cell parameters of the katoite obtained by hydration of our ferrites extracted (AcA) from the industrial clinker both in pure water and in calcium hydroxide solution. Here, the iron content  $x$  is calculated using equation 20. The  $\text{SiO}_2/\text{Al}_2\text{O}_3$  ratio  $y$  is extracted from microprobe measurements. The  $\text{SiO}_2$  and  $\text{H}_2\text{O}$  contents are then directly derived from these values.

**Table 5**

Al/Fe ratios of ferrites with the corresponding cell parameters and the coefficient of the structural formulas of katoites ( $\text{C}_3\text{A}_{(1-x)}\text{F}_x\text{S}_{y(1-x)}\text{H}_{6-2y(1-x)}$ ) related to the  $\text{Fe}_2\text{O}_3$ ,  $\text{SiO}_2$ ,  $\text{H}_2\text{O}$  contents. For AcA residues,  $w/c = 400$  after 7 days of hydration.

		Cell parameter a (Å)	$\text{Fe}_2\text{O}_3$ x	$\text{SiO}_2$ y(1-x)	$\text{H}_2\text{O}$ 6-2y(1-x)
	Katoite (ICSD n°82404)	12.5695 (11)	0	0	6
Solution	Ferrite (Al/Fe)				
Pure water	0.69 (SR0 C)	12.5400 (2)	0.28	0.28	5.44
	0.71 (SR0 A)	12.5448 (2)	0.32	0.28	5.45
	0.87 (SR3 B)	12.5215 (2)	0.11	0.24	5.51
	0.95 (SR3 D)	12.5398 (1)	0.23	0.25	5.50
Calcium hydroxide solution	0.69 (SR0 C)	12.6252 (2)	0.60	0.16	5.69
	0.71 (SR0 A)	12.6247 (2)	0.61	0.16	5.68
	0.87 (SR3 B)	12.6173 (3)	0.51	0.13	5.73
	0.95 (SR3 D)	12.6215 (2)	0.37	0.20	5.59

#### 4.4.3. The case of the ferrihydrite gel $\text{FH}_3$

The stoichiometric equation 7 shows that the iron content in katoite is closely linked to the portlandite consumption, which drives the hydroxide  $\text{FH}_3$  production. In the literature, most authors claim that  $\text{FH}_3$  gel is not visible by XRD. However, the amorphous halos of  $\text{FH}_3$  gel (Fig. 10) is observed for ferrite samples with Al/Fe ratio  $r = 0.9$  and 1, hydrated in pure water. The two broad diffuse halos around  $33^\circ$  and  $61^\circ$  ( $\text{CuK}\alpha$ ) appear clearly and correspond perfectly to the characteristic positions of ferrihydrite [66-68].

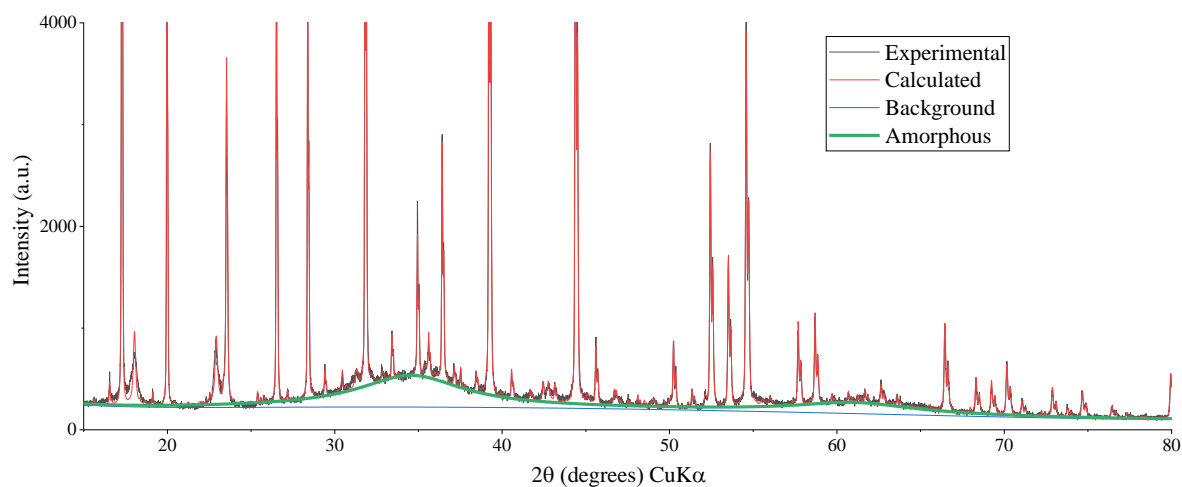


**Fig. 10.** Amorphous halos in the XRD pattern of ferrite (Al/Fe = 1) hydrated in pure water for 7 days,  $w/c = 400$

In the following, the reactivity of ferrite in solution that initially contains gypsum, i.e. sulfate ions, was investigated. As previously, we will consider successively solutions without and with portlandite.

#### 4.5. Hydration of ferrite in a gypsum saturated solution

A simplified equation of  $C_4AF$  hydration in gypsum saturated solution is given by eq.13, where  $x$  is here related to iron incorporation in ettringite ( $C_6A_{1-x}F_x\bar{S}_3H_{32}$ ). Here, ettringite replaces katoite compared to the previous case. To study the effect of sulfates on the hydration of ferrite, all the ferrite samples, both synthetic and industrial, were hydrated for seven days in a gypsum saturated solution ( $w/c = 400$ ), without a solid reservoir of gypsum. This concentration corresponds to a  $\bar{S}/A = 2.3$  molar ratio. This concentration was chosen to allow high ettringite precipitation. The initial solution contains no solid sulfate: this choice makes it possible to be sure that all the initial sulfate ions are already in solution. The only dissolution effects that could then be observed in the experiments are due solely to the ferrite dissolution.

Quantitative XRD Rietveld analysis was performed (Fig. 11 and Fig. 12) with a particular focus on the major phases: the initial ferrite and the final hydrated ettringite. Katoite and calcium monosulfoaluminate are never observed. Conductivity as a function of time for ferrites in a gypsum saturated solution is displayed, as shown in **Fig. 13**. The behavior of the synthetic and industrial ferrites also appears quite different both in XRD and in conductimetry experiments.

##### 4.5.1. Synthetic ferrites

For synthetic ferrites hydrated with the Al/Fe atomic ratio  $r$  ranging between 0 and 0.8, XRD shows that ferrite remains the main phase, with a few percent of ettringite. However, for synthetic ferrites with an Al/Fe ratio  $r > 0.8$ , an inversion of the phases is observed and ettringite becomes the main phase after 7 days in a gypsum saturated solution. This is confirmed by the calcium and sulfur concentration measurements given in **Table 6**. The sulfur concentration decreases with respect to the Al/Fe atomic ratio  $r$  and becomes very small above  $r > 0.8$ , meaning that most of the sulfate atoms are consumed by ettringite. The same applies for the calcium concentration. As already observed for the hydration in pure water at the same  $w/c = 400$  ratio, we get here a pivot value at the Al/Fe ratio  $r \approx 0.9$ , to be compared to  $r \approx 0.7$  observed in pure water.

Let us now consider the conductimetry experiments (Fig. 13A). Almost no evolution of the conductivity is observed for Al/Fe ratios  $r < 0.9$ , which is consistent with the pivot value observed with XRD. The two conductivity curves for  $r = 0.9$  and 1 are similar except regarding the time scale. A sharp decrease in conductivity can be observed during the first days (part I), followed by a progressive rise and then a gently descending plateau (part II) with a sharp drop in between. In part I, the decrease is related to the precipitation of ettringite, which consumes  $Ca^{2+}$ ,  $HO^-$ ,  $SO_4^{2-}$  ions from the sulfated solution and  $Al^{3+}$  and  $Fe^{3+}$  ions from the dissolution of ferrite. In part II, the conductivity increase is related to the dissolution of some solid phases. Usually, the dissolution of ettringite is observed when the solution runs out of sulfate, then leading to a precipitation of calcium monosulfoaluminate [12, 13, 17, 24]. Insofar as no calcium monosulfoaluminate is observed here, a re-dissolution of ettringite is precluded. Next, due to the lack of an initial solid sulfate phase, the only phase that can dissolve is the ferrite phase.

#### 4.5.2. Industrial ferrites

Looking at **Fig. 12**, it appears that the four industrial ferrites are nearly completely hydrated. The transformation from ferrite to ettringite appears at a lower Al/Fe ratio than in synthetic ferrite: with an Al/Fe ratio of about 0.7, the transformation is almost complete, with less than 5 wt.% of residual ferrite. For industrial ferrites (**Fig. 13B**), a sharp decrease in conductivity is observed the first day, followed by a plateau. Like for synthetic ferrites, the drop in conductivity can be explained by the fast precipitation of ettringite. When sulfate ions are consumed, the deviation from equilibrium is lesser and it slows the precipitation. Aluminum concentration is very low compared to sulfate concentration, which remains high, and ferrite is still present, as shown by XRD. The dissolution of ferrite is incomplete, and not all sulfate ions are consumed, in contrast to what happens with synthetic ferrites. This very low aluminum concentration, also observed on gypsum/C<sub>3</sub>A systems, is due to the fact that the system is very close to the ettringite solubility [69]. Usually, for hydration in solutions of pure water, calcium hydroxide solution, and gypsum and portlandite saturated solution, the industrial ferrites are more reactive than the synthetic ones, owing to various parameters, among which the large surface area seems to be important. It is not the case here. This system is the only one where industrial ferrites seem to display a particular behavior.

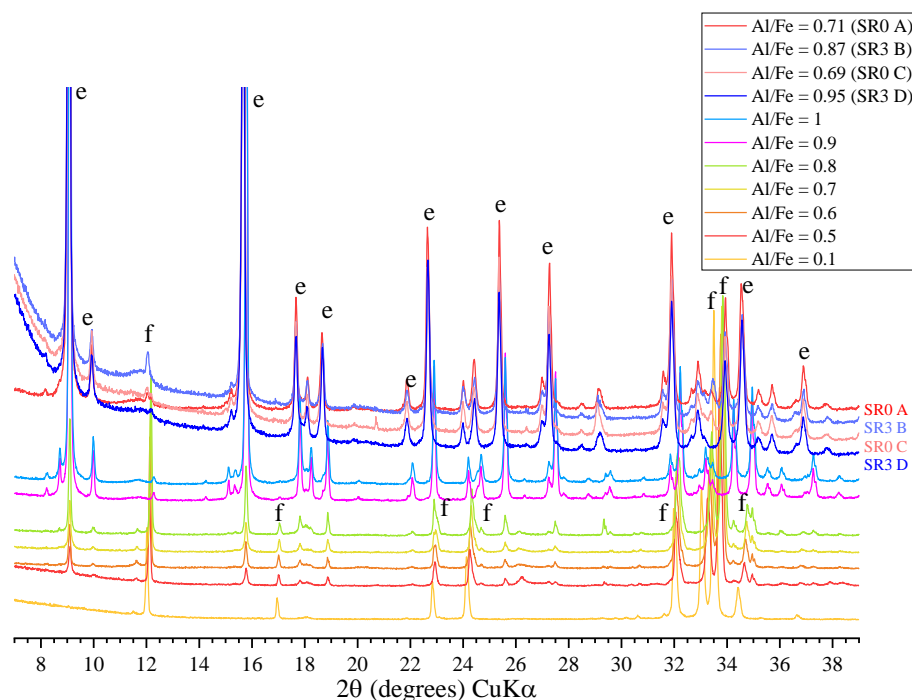


**Fig. 11.** XRD patterns of ferrites hydrated for 7 days in a gypsum saturated solution (f: ferrite, e: ettringite)

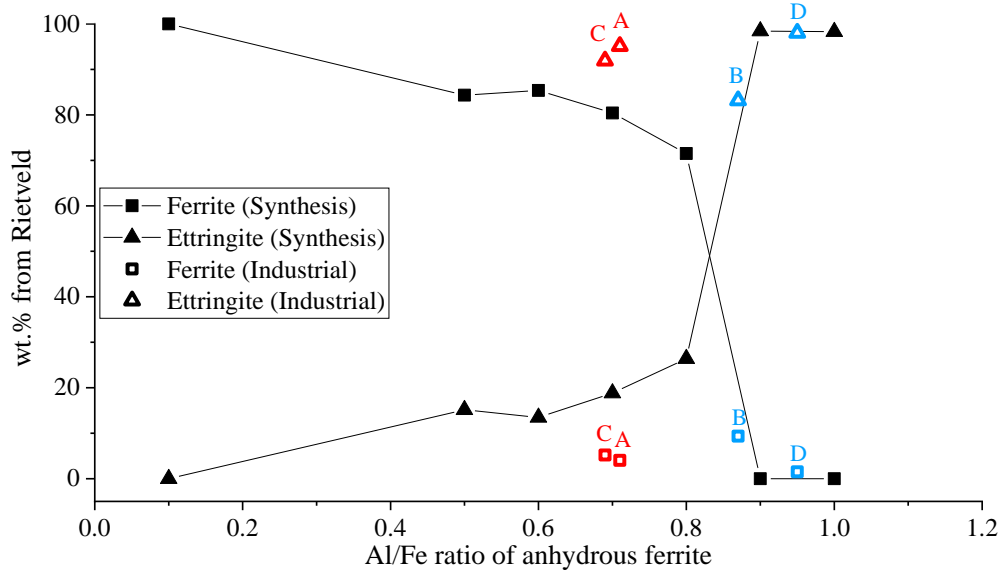


**Fig. 12.** Amount of undissolved ferrite (squares) and precipitated ettringite (triangles) after 7 days in a solution saturated with gypsum,  $w/c = 400$

**Table 6**

Calcium, aluminum, and sulfur concentrations after 7 days in a solution saturated with gypsum,  $w/c = 400$

Al/Fe	Ca (mmol/l)	Al (mmol/l)	S (mmol/l)
0.1	14.41	Very low	12.94
0.5	14.39	Very low	12.88
0.6	14.41	Very low	12.94
0.7	13.54	Very low	12.09
0.8	12.70	Very low	11.03
0.9	2.22	0.32	0.21
1	1.60	0.96	0.05
0.69 (SR0 C)	5.08	Very low	3.45
0.71 (SR0 A)	3.63	Very low	2.04
0.87 (SR3 B)	4.36	Very low	3.38
0.95 (SR3 D)	3.20	Very low	1.17

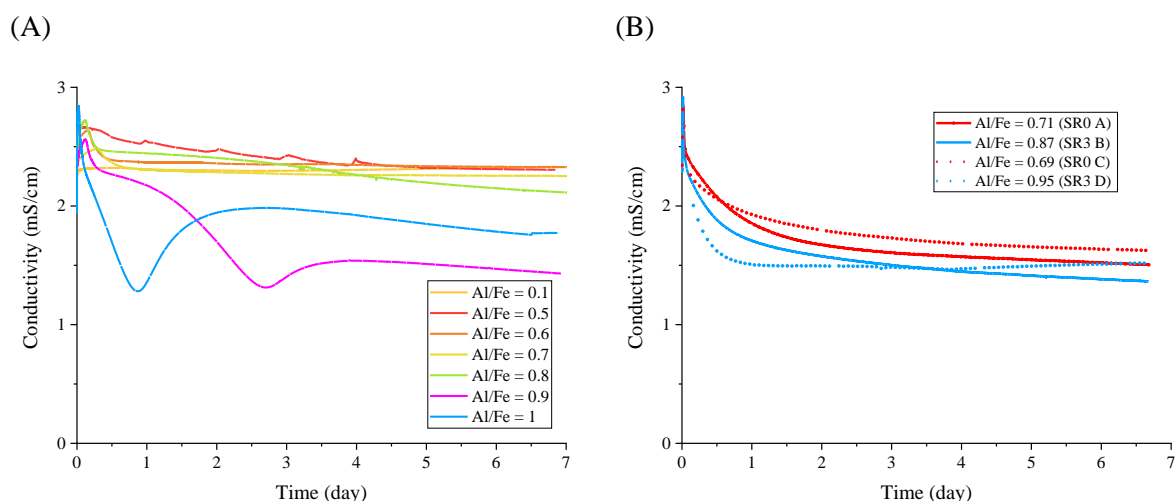


**Fig. 13.** Evolution of the conductivity for synthetic ferrites (A) and AcA residues (B) in a gypsum saturated solution,  $w/c = 400$

#### 4.6. Hydration of ferrite with a gypsum and portlandite saturated solution

##### 4.6.1. Synthetic ferrites

After having studied the effect of sulfates on ferrite hydration, we will now compare it with a gypsum and portlandite saturated solution, here also without a solid reservoir.

Over the 7 days of the experiment, the evolution of conductivity for all the synthetic ferrites is rather similar (Fig. 14), with slowly decreasing conductivity. Rietveld quantitative analyses of hydrated synthetic ferrites (Fig. 15) show that about 50 wt.% of ferrite is hydrated at the end of this period, and ettringite now represents about 50 wt.%. Approximately 35 - 50 mol.% of the initial sulfate has reacted with ferrite (Table 7) at the end of the experiment, therefore showing that the reaction is still ongoing. Next, adding portlandite to the solution has a retardation effect on the hydration of ferrite, compared to a gypsum saturated solution without portlandite. This has already been observed by previous authors [17, 19]. The same behavior is observed for all synthetic ferrite samples.

##### 4.6.2. Industrial ferrites

Here, the evolution of conductivity is not very different from the evolution observed for synthetic ferrites. It appears to be a little faster (about twice as much), with a plateau at 6 days for ferrites SR3 B, SR0 C and SR3 D, meaning that the hydration of ferrite is nearly complete in these cases. Here, the distinction between SR0 and SR3 samples is hard to make. The behavior of ferrite SR0 A is slightly different, with a shallower slope and no plateau at 6 days, which means that the hydration is slower and still not completely achieved. This is confirmed by a dosage of the solution (Table 7) where remaining sulfate ions are found in solution A unlike in the other three (B, C and D) solutions. XRD confirms these results: ferrite SR0 A, hydrated for seven days, still contains 30 wt.% of anhydrous ferrite. As previously, the difference in behavior between industrial and synthetic ferrite can be partially explained by the comparative difference in surface area.



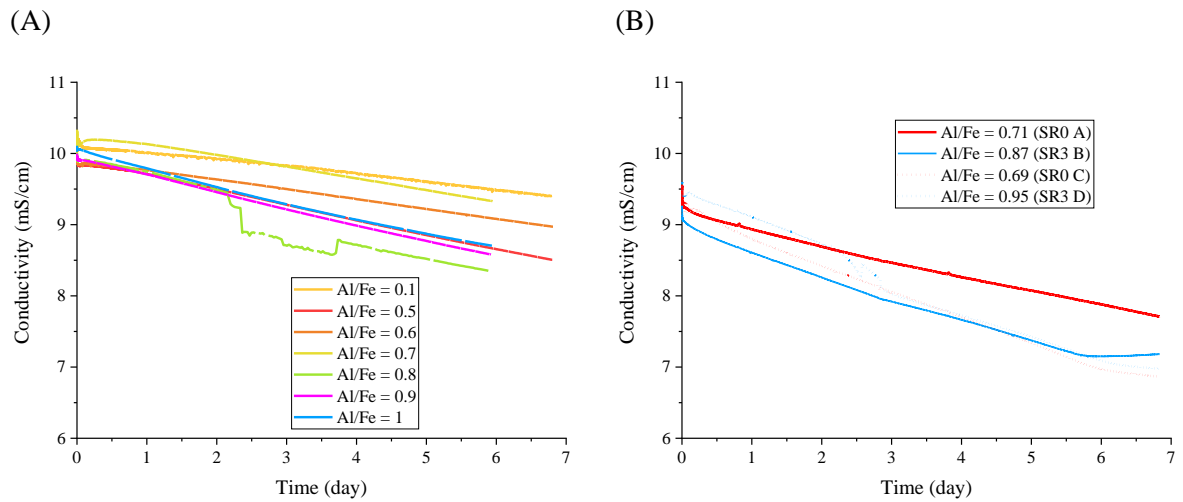


**Fig. 14.** Evolution of the conductivity of synthetic ferrites (A) and AcA residues (B) in a gypsum and portlandite saturated solution, w/c = 400

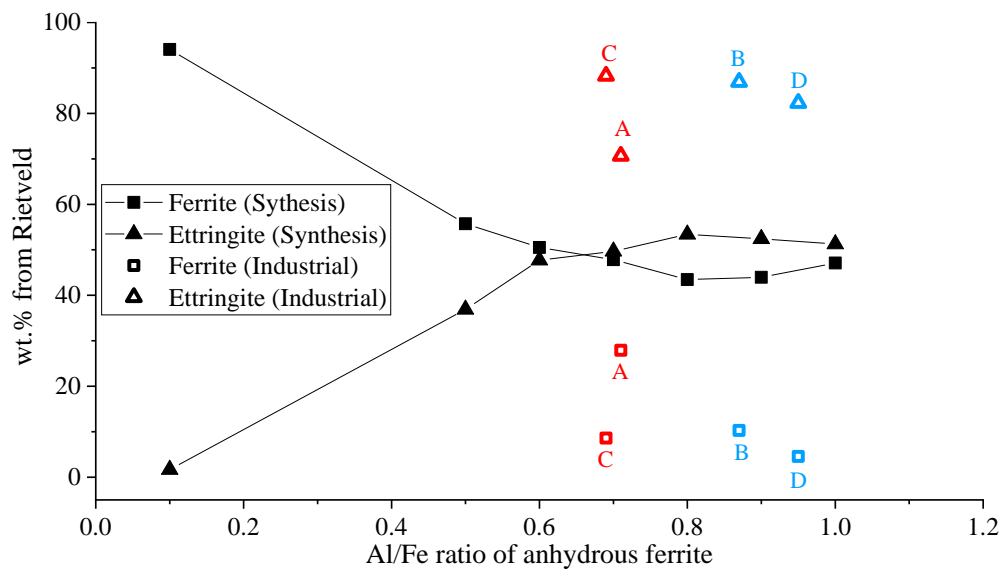


**Fig. 15.** Amount of undissolved ferrite (squares) and formed ettringite (triangles) after 7 days in a gypsum and portlandite saturated solution, w/c = 400

**Table 7**

Calcium, aluminum, and sulfur concentrations after 7 days in a gypsum and portlandite saturated solution, w/c = 400

Al/Fe	Ca (mmol/l)	Al (mmol/l)	S (mmol/l)
0.1	27.29	Very low	9.49
0.5	24.90	Very low	8.29
0.6	25.47	Very low	7.78
0.7	24.25	Very low	7.87
0.8	23.64	Very low	7.45
0.9	24.79	Very low	7.87
1	24.13	Very low	7.55

0.69 (SR0 C)	13.53	Very low	0.03
0.71 (SR0 A)	19.50	Very low	3.15
0.87 (SR3 B)	15.37	Very low	0.03
0.95 (SR3 D)	13.83	Very low	0.04

#### 4.7. Al-Fe ettringite solid solution

The incorporation of iron in ettringite was previously studied by XRD [58] and Raman spectroscopy [57] but only a few papers have studied iron incorporation in ettringite during the hydration of ferrite [20, 54]. Katoite crystallizes into octahedral-like crystals (Fig. 16A), whereas ettringite crystallizes into needle-like crystals (Fig. 16B), which makes ettringite very sensitive to preferential orientation. Therefore, XRD precise interpretation is more difficult and prevents a precise site occupancy refinement. It is therefore useful to find another solution.

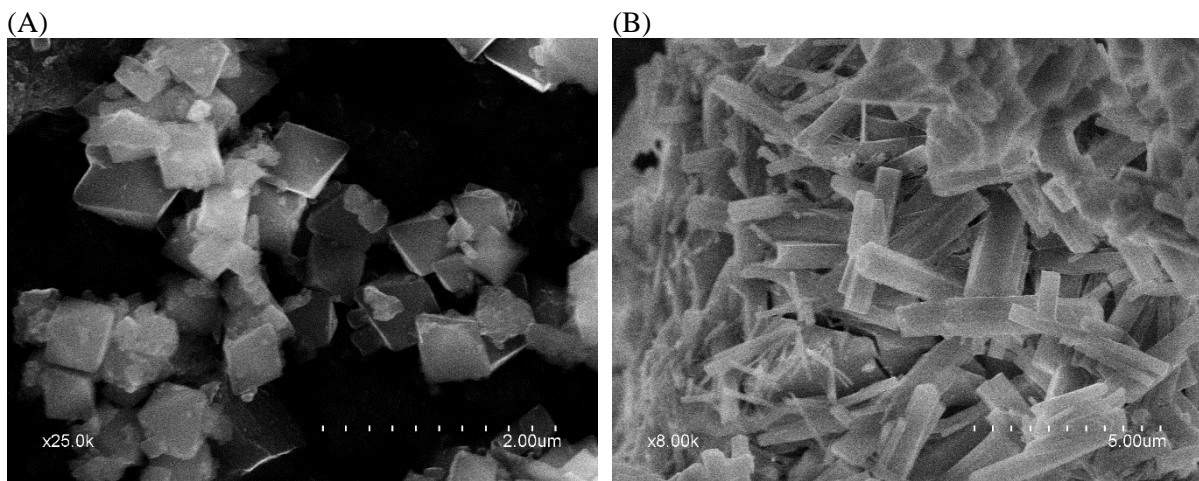


**Fig. 16.** SEM images of katoite, from  $C_4AF$  hydrated for 7 days in pure water (A) and ettringite, from ferrite ( $Al/Fe = 0.5$ ) hydrated for 28 days with gypsum (B)

Fig. 17 presents the evolution of the unit cell parameter of the final ettringite as a function of the iron content of the initial ferrite. For the gypsum and portlandite saturated solution, a roughly linear increase of the  $c$  parameter can be observed as a function of the iron content. The higher cell parameter at higher iron content may be interpreted as a higher iron incorporation. This is similar to what is observed for solutions without sulfates, where calcium hydroxide also favors iron incorporation in katoite. Such behavior is not observed for the solutions without calcium hydroxide. Here, the unit cell parameter remains constant in a wide concentration domain, and the iron incorporation in ettringite remains lower.

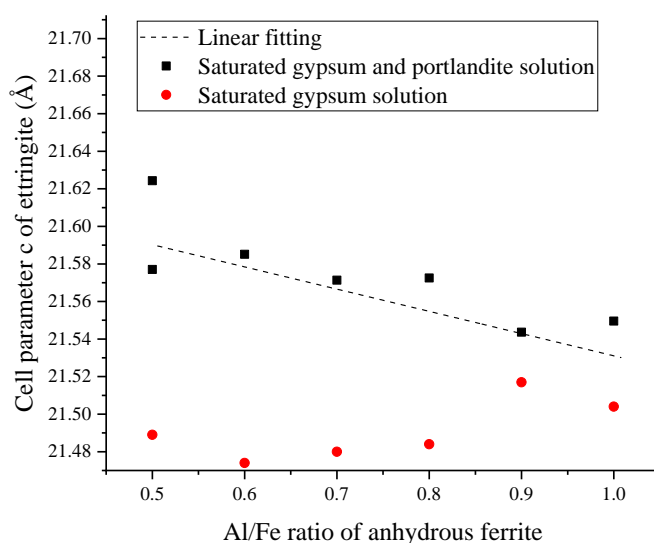


**Fig. 17.** Cell parameter  $c$  of ettringite as a function of the Al/Fe atomic ratio of ferrite

## 5. Conclusion

In this paper, the intrinsic reactivity of industrial and synthetic ferrite was investigated. Thanks to the use of conductivity in diluted solution, ICP, and XRD, it was possible to monitor very precisely the reactivity of ferrites.

The study of the reactivity using SAM and AcA residues confirms the need to dissolve the sulfates (AcA) from industrial ferrites in order to investigate the intrinsic ferrite reactivity. Indeed, sulfate proportions are very different from one residue to another, leading to unwanted reactions, independently of the nature of the ferrite. The presence of the  $C_3A$  phase in SAM residues impedes data interpretation because its dissolution rate is higher than that of ferrite.

There is an important difference in reactivity between industrial and synthetic ferrites. This can be explained by very different specific surface areas, impurities, and microstructure. However, studies with synthetic compounds enables progress to be made in the understanding of ferrite reactivity. It is also essential to study the industrial materials in order to understand the actual hydration process of ferrite.

The results show that the Al/Fe ratio and the chemical environment are fundamental parameters which help drive the ferrite hydration process. The reactivity of SR0 and SR3 ferrites can be distinguished only by their dissolution rate. For synthetic ferrites, it can be observed that there is a pivot value of the Al/Fe ratio at which there is no hydration. This value varies with the chemical environment. However, in calcium hydroxide solution, whenever the ferrite contains aluminum, hydration is observed.

Iron incorporation in katoite and ettringite was confirmed by XRD. The iron proportion in hydrates is dependent on the Al/Fe ratio of anhydrous ferrite and the amount of calcium hydroxide available in solution. For katoite, which is cubic, the results confirm Taylor's formula in calcium hydroxide solution for the whole solid solution range. For the more complex case of ettringite, the iron incorporation could not be precisely quantified.  $FH_3$  gel can also be identified by XRD when it is present in significant proportions.

Overall, ferrite can no longer be ignored and needs to be taken into account in addition to  $C_3A$ . This justifies durability studies as a function of environmental classes.

## 6. Acknowledgments

This work was supported by SFIC (Syndicat Français de l'Industrie Cimentière, now France Ciment) and ANRT (Association Nationale de la Recherche et de la Technologie), under the CIFRE contract 2019/0803. The authors thank Yannick Demeusy for the study on synthetic ferrite. We acknowledge the support of the X-ray crystallography facility, DIFFRAX Ecole polytechnique, Institut Polytechnique de Paris.

## 7. References

- [1] E.T. Carlson, P.H. Bates, Can cement durability be predicted?, *Engineering News-Record*, 107 (1931) 130-132
- [2] T. Thorvaldson, Chemical aspects of the durability of cement products, in: 3th International Symposium on the Chemistry of Cement London, UK, 1952, pp. 437-467.
- [3] A. Mériot, M.-N. de Noirfontaine, M. Courtial, L. Izoret, S. Tusseau-Nenez, M. Labourel, S. Gauffinet, F. Dunstetter, From selective dissolution to crystal chemistry of brownmillerite in sulfate resisting cement, *Journal of the American Ceramic Society*, 106 (2023) 709-721. <https://doi.org/10.1111/jace.18764>
- [4] H.F.W. Taylor, *Cement Chemistry*, 2nd edition, Thomas Telford Edition, London, 1997.
- [5] D. Wan, W. Zhang, Y. Tao, Z. Wan, F. Wang, S. Hu, Y. He, The impact of Fe dosage on the ettringite formation during high ferrite cement hydration, *Journal of American Ceramic Society*, 104 (2021) 3652-3664. <https://doi.org/10.1111/jace.17640>
- [6] X. Huang, F. Wang, S. Hu, Y. Lu, M. Rao, Y. Mu, Brownmillerite hydration in the presence of gypsum: the effect of Al/Fe ratio and sulphate ions, *Journal of the American Ceramic Society*, 102 (2019) 5545-5554. <https://doi.org/10.1111/jace.16384>
- [7] T. Hertel, J. Neubauer, F. Goetz-Neuhoeffer, Study of hydration potential and kinetics of the ferrite phase in iron-rich CAC, *Cement and Concrete Research*, 83 (2016) 79-85. <https://doi.org/10.1016/j.cemconres.2016.01.004>
- [8] H. Zhong, K. Zhang, L. Yang, F. Wang, S. Hu, M. Lv, J. He, In-depth understanding the hydration process of Mn-containing ferrite: A comparison with ferrite, *Journal of the American Ceramic Society*, 105 (2022) 4883-4896. <https://doi.org/10.1111/jace.18444>
- [9] K. Sotiriadis, R. Mroz, P. Macova, A.S. Mazur, A. Krajnc, Long-term sulfate resistance of synthesized cement systems with variable C<sub>3</sub>A/C<sub>4</sub>AF ratio at low temperature or ambient conditions: Insights into the crystalline and amorphous phase assemblage, *Cement and Concrete Research*, 160 (2022). <https://doi.org/10.1016/j.cemconres.2022.106902>
- [10] G. Le Saoût, D. Lafon-Pham, J.C. Roux, Hydration of a calcium sulfoaluminate cement blended with zincite, *Advances in Cement Research*, 33 (2021) 183-191. <https://doi.org/10.1680/jadcr.19.00136>
- [11] J. Rose, A. Bénard, S. El Mrabet, A. Masion, I. Moulin, V. Briois, L. Olivi, J.-Y. Bottero, Evolution of iron speciation during hydration of C<sub>4</sub>AF, *Waste Management*, 26 (2006) 720-724. <https://doi.org/10.1016/j.wasman.2006.01.021>
- [12] N. Meller, C. Hall, A.C. Jupe, S.L. Colston, S.D.M. Jacques, P. Barnes, J. Phipps, The paste hydration of brownmillerite with and without gypsum: a time resolved synchrotron diffraction study at 30, 70, 100 and 150 °C, *Journal of Materials Chemistry*, 14 (2004) 428-435. <https://doi.org/10.1039/B313215C>
- [13] V.S. Ramachandran, J.J. Beaudoin, Hydration of C<sub>4</sub>AF + gypsum: study of various factors, in: 7th International Congress on the Chemistry of Cement, Paris, France, 1980, pp. 25-30.
- [14] K.L. Scrivener, P.L. Pratt, Microstructural studies of the hydration of C<sub>3</sub>A and C<sub>4</sub>AF independently and in cement paste, *Materials Research Society Symposia Proceedings*, 31 (1984) 207-219

- [15] A. Cuesta, I. Santacruz, S.G. Sanf elix, F. Fauth, M.A.G. Aranda, A.G. de La Torre, Hydration of C<sub>4</sub>AF in the presence of other phases: a synchrotron X-ray powder diffraction study, *Construction and Building Materials*, 101 (2015) 818-827. <https://doi.org/10.1016/j.conbuildmat.2015.10.114>
- [16] D. Ectors, J. Neubauer, F. Goetz-Neunhoeffler, The hydration of synthetic brownmillerite in presence of low Ca-sulfate content and calcite monitored by quantitative in-situ-XRD and heat flow calorimetry, *Cement and Concrete Research*, 54 (2013) 61-68. <https://doi.org/10.1016/j.cemconres.2013.08.011>
- [17] M. Collepardi, S. Monosi, G. Moriconi, M. Corradi, Tetracalcium-aluminoferrite hydration in the presence of lime and gypsum, *Cement and Concrete Research*, 9 (1979) 431-437. [https://doi.org/10.1016/0008-8846\(79\)90040-1](https://doi.org/10.1016/0008-8846(79)90040-1)
- [18] J.M. Fortune, J.M.D. Coey, Hydration products of calcium aluminoferrite, *Cement and Concrete Research*, 13 (1983) 696-702. [https://doi.org/10.1016/0008-8846\(83\)90060-1](https://doi.org/10.1016/0008-8846(83)90060-1)
- [19] E.T. Carlson, Action of water on calcium aluminoferrites, *Journal of Research of the National Bureau of Standards*, 68A (1964) 453-463. <https://doi.org/10.6028/jres.068A.044>
- [20] A. Emanuelson, S. Hansen, E. Henderson, A. Landa-Canova, S. E., Ferrite microstructure in clinker and hydration of synthetic phases and sulphate resisting cements, in: 10th International Congress on the Chemistry of Cement, G teborg, Sweden, 1997, pp. li060.
- [21] A. Negro, L. Montanaro, A. Bachiorrini, On the hydration of ferrite phase in the presence of lime and gypsum, in: 8th International Congress on the Chemistry of Cement, Rio de Janeiro, Brazil, 1986, pp. 394-400.
- [22] L. Montanaro, A. Negro, Expansion de la phase ferrite en pr sence de gypse et chaux : comparaison avec l'aluminate tricalcique, *Cement and Concrete Research*, 18 (1988) 812-818. [https://doi.org/10.1016/0008-8846\(88\)90107-X](https://doi.org/10.1016/0008-8846(88)90107-X)
- [23] N. Meller, C. Hall, J. Crawshaw, ESEM evidence for through-solution transport during brownmillerite hydration, *Journal of Material Science*, 39 (2004) 6611-6614. <https://doi.org/10.1023/B:JMSC.0000044904.51813.74>
- [24] W.L. de Keyser, Travaux ex cut s sous l' gide du comit  de la recherche fondamentale du CRIC, Comit  Technique CT1 "Etudes Fondamentales des Ciments", (1965) 46-76
- [25] D. Ectors, F. Goetz-Neunhoeffler, C.M. Neubauer, Hydration of synthetic brownmillerite in an Portland cement near environment, in: 1<sup>st</sup> International Conference on the Chemistry of Construction Materials (ICCCM 1), Berlin, Germany, 2013.
- [26] M. Fukuhara, S. Goto, K. Asaga, M. Daimon, R. Kondo, Mechanisms and kinetics of C<sub>4</sub>AF hydration with gypsum, *Cement and Concrete Research*, 11 (1981) 407-414. [https://doi.org/10.1016/0008-8846\(81\)90112-5](https://doi.org/10.1016/0008-8846(81)90112-5)
- [27] J.-P. Perez, Etude de l'hydratation des phases constitutives d'un ciment Portland et de la r sistance m canique des p tes pures et mortiers : influence des trialcanolamines, in, Universit  de Bourgogne, Dijon, France, 2002.
- [28] W.L. de Keyser, N. Tenoutasse, The hydration of the ferrite phase of cements, in: 5th International Symposium on the Chemistry of Cement, Tokyo, Japan, 1968, pp. 379-386.
- [29] H. Zhong, L. Yang, F. Wang, Understanding the adsorption of calcium sulfate on tetracalcium aluminoferrite and tricalcium aluminate surfaces, *Journal of American Ceramic Society*, 106 (2023) 7596-7610. <https://doi.org/10.1111/jace.19350>
- [30] C. Plowman, J.G. Cabrera, Mechanism and kinetics of hydration of C<sub>3</sub>A and C<sub>4</sub>AF, extracted from cement, *Cement and Concrete Research*, 14 (1984) 238-248. [https://doi.org/10.1016/0008-8846\(84\)90110-8](https://doi.org/10.1016/0008-8846(84)90110-8)
- [31] H. Wang, D. de Leon, H. Farzam, C<sub>4</sub>AF reactivity-chemistry and hydration of industrial cement, *ACI Materials Journal*, 111 (2014) 201-210. <https://doi.org/10.14359/51686504>
- [32] P.E. Stutzman, P. Feng, J.W. Bullard, Phase analysis of Portland cement by combined quantitative X-Ray powder diffraction and scanning electron microscopy, *Journal of Research of the National Institute of Standards and Technology*, 121 (2016) 47-107. <https://doi.org/10.6028/jres.121.004>
- [33] D. Damidot, A. Nonat, A method for determining the advancement of the hydration of C<sub>3</sub>S in diluted suspensions by means of simultaneous conductimetric and calorimetric measurements, in: 9<sup>th</sup> International Congress on the Chemistry of Cement, New Delhi (India), 1992, pp. 227-233.
- [34] D. Damidot, A. Nonat, P. Barret, Kinetics of tricalcium silicate hydration in diluted suspensions by microcalorimetric measurements, *Journal of the American Ceramic Society*, 73 (1990) 3319-3322

- [35] S. Garrault-Gauffinet, A. Nonat, Experimental investigation of calcium silicate hydrate (C-S-H) nucleation, *Journal of Crystal Growth*, 200 (1999) 565-574. [https://doi.org/10.1016/S0022-0248\(99\)00051-2](https://doi.org/10.1016/S0022-0248(99)00051-2)
- [36] L. Nicoleau, A. Nonat, D. Perrey, The di- and tricalcium silicate dissolutions, *Cement and Concrete Research*, 47 (2013) 14-30. <https://doi.org/10.1016/j.cemconres.2013.01.017>
- [37] L. Nicoleau, E. Schreiner, A. Nonat, Ion-specific effects influencing the dissolution of tricalcium silicate, *Cement and Concrete Research*, 59 (2014) 118-138. <http://dx.doi.org/10.1016/j.cemconres.2014.02.006>
- [38] C. Nalet, A. Nonat, Effects of hexitols on the hydration of tricalcium silicate, *Cement and Concrete Research*, 91 (2017) 87-96. <https://doi.org/10.1016/j.cemconres.2016.11.004>
- [39] AFNOR, Ciments. Partie 1 Composition, spécifications et critères de conformité des ciments courants, in, 2012.
- [40] R.W. Cheary, A. Coelho, A fundamental parameters approach to X-ray line-profile fitting, *Journal of Applied Crystallography*, 25 (1992) 109-121. <https://doi.org/10.1107/S0021889891010804>
- [41] W.A. Dollase, Correction of intensities for preferred orientation in powder diffraction: application of the March Model, *Journal of Applied Crystallography*, 19 (1986) 267-272. <https://doi.org/10.1107/S0021889886089458>
- [42] A.A. Colville, S. Geller, The crystal structure of brownmillerite,  $\text{Ca}_2\text{FeAlO}_5$ , *Acta Crystallographica B*, 27 (1971) 2311-2315. <https://doi.org/10.1107/S056774087100579X>
- [43] A.A. Colville, The crystal structure of  $\text{Ca}_2\text{Fe}_2\text{O}_5$  and its relation to the nuclear electric field gradient at the iron sites, *Acta Crystallographica B*, 26 (1970) 1469-1473. <https://doi.org/10.1107/S056774087000434X>
- [44] P. Mondal, J.W. Jeffery, The crystal structure of tricalcium aluminate,  $\text{Ca}_3\text{Al}_2\text{O}_6$ , *Acta Crystallographica B*, 31 (1975) 689-697. <https://doi.org/10.1107/S0567740875003639>
- [45] G.A. Lager, R.B. Von Dreele, Neutron powder diffraction study of hydrogarnet to 9.0 GPa, *American Mineralogist*, 81 (1996) 1097-1104. <https://doi.org/10.2138/am-1996-9-1006>
- [46] F. Goetz-Neunhoffer, J. Neubauer, Refined ettringite ( $\text{Ca}_6\text{Al}_2(\text{SO}_4)_3(\text{OH})_{12}\cdot 26\text{H}_2\text{O}$ ) structure for quantitative X-ray diffraction analysis, *Powder Diffraction*, 21 (2006) 4-11. <https://doi.org/10.1154/1.2146207>
- [47] R. Allmann, Refinement of the hydrid layer structure  $\text{Ca}_2\text{Al}(\text{OH})_6\cdot\frac{1}{2}\text{SO}_4\cdot 3\text{H}_2\text{O}$ , *Neues Jahrbuch für Mineralogie Monatshefte*, 2017 (1977) 136-144
- [48] J.C.A. Boeyens, V.V.H. Ichharam, Redetermination of the crystal structure of calcium sulphate dihydrate,  $\text{CaSO}_4\cdot 2\text{H}_2\text{O}$ , *Zeitschrift für Kristallographie*, 217 (2002) 9-10. <https://doi.org/10.1524/ncrs.2002.217.1.9>
- [49] Y. Tao, D. Wan, W. Zhang, F. Wang, S. Hu, Intrinsic reactivity and dissolution characteristics of tetracalcium aluminoferrite, *Cement and Concrete Research*, 146 (2021) 106485. <https://doi.org/10.1016/j.cemconres.2021.106485>
- [50] F. Pertlik, Bibliography of hibschite, a hydrogarnet of grossular type, *GeoLines*, 15 (2003) 113-119
- [51] J.A. Rickerby, Characterisation of hardened cements incorporating simulant intermediate level waste in, University of Leeds, UK, 2015.
- [52] B.Z. Dilnesa, B. Lothenbach, G. Renaudin, A. Wichser, D. Kulik, Synthesis and characterization of hydrogarnet  $\text{Ca}_3(\text{Al}_x\text{Fe}_{1-x})_2(\text{SiO}_4)_y(\text{OH})_{4(3-y)}$ , *Cement and Concrete Research*, 59 (2014) 96-111. <https://doi.org/10.1016/j.cemconres.2014.02.001>
- [53] E.T. Carlson, Some properties of the calcium aluminoferrite hydrates, National Institute of Standards and Technology, Building Science Series 6 (1966) 01-11. <https://doi.org/10.6028/NBS.BSS.6>
- [54] A. Emanuelson, S. Hansen, Distribution of iron among ferrite hydrates, *Cement and Concrete Research*, 27 (1997) 1167-1177. [https://doi.org/10.1016/S0008-8846\(97\)00120-8](https://doi.org/10.1016/S0008-8846(97)00120-8)
- [55] R.S. Gollop, H.F.W. Taylor, Microstructural and microanalytical studies of sulfate attack. II. Sulfate resisting Portland cement: ferrite composition and hydration chemistry, *Cement and Concrete Research*, 24 (1994) 1347-1358. [https://doi.org/10.1016/0008-8846\(94\)90120-1](https://doi.org/10.1016/0008-8846(94)90120-1)
- [56] D. Damidot, F.P. Glasser, Thermodynamic investigation of the  $\text{CaO}-\text{Al}_2\text{O}_3-\text{CaSO}_4-\text{H}_2\text{O}$  system at 25°C and influence of  $\text{Na}_2\text{O}$ , *Cement and Concrete Research*, 23 (1993) 221-238. [https://doi.org/10.1016/0008-8846\(93\)90153-Z](https://doi.org/10.1016/0008-8846(93)90153-Z)



- [57] G. Renaudin, R. Segni, D. Mentel, J.-M. Nedelec, F. Leroux, C. Tavio-Gheho, A Raman study of the sulfated cement hydrates: ettringite and monosulfoaluminate, *Journal of Advanced Concrete Technology*, 5 (2007) 299-312. <https://doi.org/10.3151/jact.5.299>
- [58] G. Möschner, B. Lothenbach, F. Winnefeld, A. Ulrich, R. Figi, R. Kretzschmar, Solid solution between Al-ettringite and Fe-ettringite ( $\text{Ca}_6[\text{Al}_{1-x}\text{Fe}_x(\text{OH})_6]_2(\text{SO}_4)_3 \cdot 26\text{H}_2\text{O}$ ), *Cement and Concrete Research*, 39 (2009) 482-489. <https://doi.org/10.1016/j.cemconres.2009.03.001>
- [59] B.Z. Dilnesa, B. Lothenbach, G. Le Saout, G. Renaudin, A. Mesbah, Y. Filinchuk, A. Wichser, E. Wieland, Iron in carbonate containing AFm phases, *Cement and Concrete Research*, 41 (2011) 311-323. <https://doi.org/10.1016/j.cemconres.2010.11.017>
- [60] A.C. Jupe, J.K. Cockcroft, P. Barnes, S.L. Colston, G. Sankar, C. Hall, The site occupation of Mg in the brownmillerite structure and its effect on hydration properties, *Journal of Applied Crystallography*, 34 (2001) 55-61. <https://doi.org/10.1107/S0021889800016095>
- [61] P. Fierens, J. Tirlocq, J.P. Verhaegen, Luminescence et hydratation du silicate tricalcique, *Cement and Concrete Research*, 3 (1973) 549-560. [https://doi.org/10.1016/0008-8846\(73\)90093-8](https://doi.org/10.1016/0008-8846(73)90093-8)
- [62] P. Juilland, E. Gallucci, R. Flatt, K. Scrivener, Dissolution theory applied to the induction period in alite hydration, *Cement and Concrete Research*, 40 (2010) 831-844. <https://doi.org/10.1016/j.cemconres.2010.01.012>
- [63] I. Jawed, S. Goto, R. Kondo, Hydration of tetracalcium aluminoferrite in presence of lime and sulfates, *Cement and Concrete Research*, 6 (1976) 441-453. [https://doi.org/10.1016/0008-8846\(76\)90073-9](https://doi.org/10.1016/0008-8846(76)90073-9)
- [64] H. Wang, H. Farzam, Importance of clinker liquid phases, particularly the ferrite phase in cement chemistry, *Journal of the Chinese Ceramic Society*, 43 (2015) 86-101. <https://doi.org/10.14062/j.issn.0454-5648.2015.10.01>
- [65] R.D. Shannon, Revised effective ionic radii and systematic studies of interatomic distances in halides and chalcogenides, *Acta Crystallographica A*, 32 (1976) 751-767. <https://doi.org/10.1107/S0567739476001551>
- [66] L. Carlson, U. Schwertmann, Natural ferrihydrites in surface deposits from Finland and their association with silica, *Geochimica et Cosmochimica Acta*, 45 (1981) 421-429. [https://doi.org/10.1016/0016-7037\(81\)90250-7](https://doi.org/10.1016/0016-7037(81)90250-7)
- [67] A. Manceau, V.A. Drits, Local structure of ferrihydrite and ferroxihite by EXAFS spectroscopy, *Clay Minerals*, 28 (1993) 165-184. <https://doi.org/10.1180/claymin.1993.028.2.01>
- [68] J. Li, T. Zeng, J. Chang, Microstructure of  $\text{Fe}(\text{OH})_3$  phase in hydration products of calcium sulfoaluminate cement, *Construction and Building Materials*, 400 (2023). <https://doi.org/10.1016/j.conbuildmat.2023.132609>
- [69] S. Pourchet, L. Regnaud, J.-P. Perez, A. Nonat, Early  $\text{C}_3\text{A}$  hydration in the presence of different kinds of calcium sulfate, *Cement and Concrete Research*, 39 (2009) 989-996. <https://doi.org/10.1016/j.cemconres.2009.07.019>